THE UNIVERSITY of EDINBURGH

Edinburgh Research Explorer

Aldh2 is a lineage-specific metabolic gatekeeper in melanocyte stem cells

Citation for published version:
Brunsdon, H, Brombin, A, Peterson, S, Postlethwait, JH & Patton, EE 2022, 'Aldh2 is a lineage-specific metabolic gatekeeper in melanocyte stem cells', *Development*. https://doi.org/10.1242/dev.200277

Digital Object Identifier (DOI):
10.1242/dev.200277

Link:
Link to publication record in Edinburgh Research Explorer

Document Version:
Publisher's PDF, also known as Version of record

Published In:
Development

General rights
Copyright for the publications made accessible via the Edinburgh Research Explorer is retained by the author(s) and / or other copyright owners and it is a condition of accessing these publications that users recognise and abide by the legal requirements associated with these rights.

Take down policy
The University of Edinburgh has made every reasonable effort to ensure that Edinburgh Research Explorer content complies with UK legislation. If you believe that the public display of this file breaches copyright please contact openaccess@ed.ac.uk providing details, and we will remove access to the work immediately and investigate your claim.

Download date: 30. Jun. 2022

Aldh2 is a lineage-specific metabolic gatekeeper in melanocyte stem cells

Hannah Brunsdon[1,2], Alessandro Brombin[1,2], Samuel Peterson[3], John H. Postlethwait[3], and E. Elizabeth Patton[1,2*]

1. MRC Human Genetics Unit, Institute of Genetics and Cancer, The University of Edinburgh, Western General Hospital Campus, Crewe Road, Edinburgh, EH4 2XU, UK.
2. Cancer Research UK Edinburgh Centre, Institute of Genetics and Cancer, The University of Edinburgh, Western General Hospital Campus, Crewe Road, Edinburgh, EH4 2XU, UK.
3. Institute of Neuroscience, University of Oregon, Eugene, OR 97403, USA

* Corresponding author: e.patton@ed.ac.uk

KEY WORDS: Melanocyte stem cell, regeneration, Aldh2, formaldehyde, metabolism, purines

SUMMARY STATEMENT

In melanocyte regeneration, quiescent McSCs respond by re-expressing a neural crest identity, followed by an Aldh2-dependent metabolic switch to generate progeny.

© 2022. Published by The Company of Biologists Ltd.
This is an Open Access article distributed under the terms of the Creative Commons Attribution License (http://creativecommons.org/licenses/by/4.0), which permits unrestricted use, distribution and reproduction in any medium provided that the original work is properly attributed.

Development • Accepted manuscript

ABSTRACT

Melanocyte stem cells (McSCs) in zebrafish serve as an on-demand source of melanocytes during growth and regeneration, but metabolic programs associated with their activation and regenerative processes are not well known. Here, using live imaging coupled with scRNA-sequencing, we discovered that during regeneration quiescent McSCs activate a dormant embryonic neural crest transcriptional program followed by an aldehyde dehydrogenase (Aldh) 2 metabolic switch to generate progeny. Unexpectedly, while ALDH2 is well known for its aldehyde clearing mechanisms, we find that in regenerating McSCs Aldh2 activity is required to generate formate – the one-carbon (1C) building block for nucleotide biosynthesis – through formaldehyde metabolism. Consequently, we find that disrupting the 1C cycle with low doses of methotrexate causes melanocyte regeneration defects. In the absence of Aldh2, we find that purines are the metabolic end product sufficient for activated McSCs to generate progeny. Together, our work reveals McSCs undergo a two-step cell state transition during regeneration, and that the reaction products of Aldh2 enzymes have tissue-specific stem cell functions that meet metabolic demands in regeneration.

INTRODUCTION

Melanocytes are pigment producing cells that provide black-brown pigmentation in the hair, skin and eyes in the animal kingdom. Melanocytes can emerge directly from the neural crest during development, while other melanocytes come from melanocyte stem cells (McSCs), that are also neural crest derived, and that replenish melanocyte populations in the adult (Mort et al. 2015). In mammals, distinct McSC populations serve as reservoirs for melanocytes that pigment the growing hair shaft, or for skin pigmentation in response to UV-irradiation or wound healing (Nishimura et al. 2005; Adameyko et al. 2009; Chou et al. 2013). In zebrafish, nerve-associated

Development • Accepted manuscript

McSCs are an on-demand regenerative population for zebrafish at all stages, and the cell-of-origin for multiple pigment cell types as the zebrafish grows to become an adult (Budi et al. 2008; Budi et al. 2011; Dooley et al. 2013; Singh et al. 2016; Brombin et al. 2022). Imaging analysis over time as well as lineage-tracing studies show McSC progeny directly give rise to pigmented melanocytes (Dooley et al. 2013; Singh et al. 2016; Brombin et al. 2022). How McSCs respond to regenerative signals to generate melanocytes is a central question for adult stem cell biology, but also for melanoma pathogenesis, which is increasingly understood to re-activate and depend upon melanocyte lineage developmental programs in disease progression (White et al. 2011; Kaufman et al. 2016; Travnickova et al. 2019; Varum et al. 2019; Johansson et al. 2020; Marie et al. 2020; Baggiolini et al. 2021).

Zebrafish are uniquely poised for studying stem cells due to their genetic tractability and amenability to advanced imaging, enabling the intricacies of stem cell and developmental lineages to be followed at the single cell resolution in living animals (Kelsh et al. 1996; Owen et al. 2020; Travnickova and Patton 2021). During zebrafish embryonic development, melanocytes that originate directly from the neural crest generate stripes along the body (Kelsh and Barsh 2011). McSCs that reside at the dorsal root ganglion (DRG) stem cell niche are also established during embryogenesis, are multi-potent, and give rise to glia and multiple pigment cell types that contribute to the adult pigmentation pattern and serve as a source for melanocytes in regeneration (Budi et al. 2008; Hultman et al. 2009; Budi et al. 2011; Johnson et al. 2011; Kelsh and Barsh 2011; Dooley et al. 2013; Singh et al. 2016; Irion and Nusslein-Volhard 2019; Brombin et al. 2022).

Recently, we identified an ErbB-dependent developmental *tfap2b*+ McSC population that we found to be distinct within neural crest and pigment cell lineages, and which lineage tracing analysis showed gave rise to all three zebrafish pigment cell types, including melanocytes, as well as nerve-associated cells (Brombin et al. 2022). Amongst members of the zebrafish Aldehyde dehydrogenase (Aldh) 1 and 2 enzyme family, which are well conserved with

Development • Accepted manuscript

analogous human enzymes, we found *aldh2* gene paralogs were specifically expressed in these *tfap2b*+ McSCs **(Fig. 1A, S1)**. Aldehyde-processing enzymes are viewed as essential clearing agents that rapidly deactivate harmful aldehydes, and also as markers of somatic and cancer stem cell populations (O'Brien et al. 2005; Marcato et al. 2011; Pontel et al. 2015; Garaycoechea et al. 2018). In the bone marrow, two specific enzymes, aldehyde dehydrogenase (ALDH) 2 and alcohol dehydrogenase (ADH) 5, protect hematopoietic stem cells (HSCs) from endogenous formaldehyde accumulation and toxicity (Dingler et al. 2020; Nakamura et al. 2020; Oka et al. 2020; Jung and Smogorzewska 2021; Mu et al. 2021). The importance of aldehyde detoxification in human biology is exemplified by the genetic variants of *ALDH2* in the human population, such as the single nucleotide polymorphism r671 in *ALDH2* (c.1510G>A; p.E504K; ALDH2*2), which confers loss-of-function in 560 million people, mainly of East Asian origin (Chen et al. 2014; Chen et al. 2020). Carriers of the r671 *ALDH2* polymorphism can experience adverse reactions to acetaldehyde from exogenous alcohol consumption and are at risk for a range of diseases including osteoporosis, cardiovascular disease, neurodegeneration, and Fanconi Anemia (Harada et al. 1981; Brooks et al. 2009; Hiura et al. 2010; Takeuchi et al. 2012; Matsuo et al. 2013; Masaoka et al. 2016; Chang et al. 2017).

Much of the toxicity from aldehydes can be attributed to metabolites such as acetaldehyde and formaldehyde, which cause mutations and chromosomal rearrangements by direct damage to DNA (Pontel et al. 2015; Garaycoechea et al. 2018). Recent work shows that a two-tier protection mechanism in cells defends against aldehyde-induced DNA crosslinks: first, aldehydes are cleared by enzymes, such as ALDH2 and ADH5, and second, replication-coupled DNA damage response pathways repair crosslinks and remove adducts (Langevin et al. 2011; Rosado et al. 2011; Garaycoechea et al. 2012; Pontel et al. 2015; Garaycoechea et al. 2018; Hodskinson et al. 2020). These studies emphasize the nature of aldehyde toxicity and homeostatic clearance, primarily investigated in the hematopoietic stem cell compartment. However, other work proposes more varied roles for aldehydes, namely that by-products

Development • Accepted manuscript

generated by aldehyde detoxification enzyme reactions also sustain essential downstream cellular metabolic processes (Jacobson and Bernofsky 1974; Bae et al. 2017; Burgos-Barragan et al. 2017). What is yet unknown is how the reaction products of aldehyde metabolism by ALDH2 contribute to the physiology of specific cells and tissues in processes other than toxicity. Here, we discover a new requirement for Aldh2-dependent metabolism in activated McSCs during regeneration.

RESULTS

A lineage-specific function for Aldh2 in melanocyte regeneration

To learn how ALDH2 functions in stem cells other than HSCs and in an intact animal, we set out to study the zebrafish McSC population in melanocyte regeneration. We employed the ALDH2 inhibitor (ALDH2i) CVT-10216 in a melanocyte regeneration assay that is dependent on a temperature sensitive splicing defect of the master melanocyte transcription factor MITF (*mitfa*^{vc7}) (Johnson et al. 2011; Zeng et al. 2015). In wild-type embryos, neural crest-derived embryonic melanocytes pigment the epidermis during the first 72 hours of development before McSCs are activated. The *mitfa*^{vc7}regeneration model allows us to bypass embryonic pigmentation by growing *mitfa*^{vc7} embryos at higher temperatures (such that *mitfa* is spliced incorrectly) to deplete Mitfa activity during this 72 hour period. After this, melanocyte regeneration can be activated from McSCs in *mitfa*^{vc7} embryos by lowering the water temperature to a level permissive for correct splicing of *mitfa*, thereby restoring its activity and allowing melanocytes to regenerate from McSCs over a period of 48 hours (Johnson et al. 2011) **(Fig. 1B)**. In zebrafish embryos grown in the presence of CVT-10216, we did not detect any discernible effects on embryonic melanocyte development. However, melanocyte regeneration from McSCs was significantly delayed in ALDH2i-treated embryos, indicating that Aldh2 has a lineage-specific function in McSCs **(Fig. 1C, Fig. S1).**

Development • Accepted manuscript

CVT-10216 is reported to have a >40-fold selectivity for ALDH2 over other ALDH enzymes (Chen et al. 2014), however, to confirm this specificity in zebrafish, we generated an *aldh2.1* - *aldh2.2* double mutant line by CRISPR-Cas9, henceforth referred to as *aldh2-/-*. The genetic similarity between these two paralogs made generating specific *aldh2* mutants difficult, so we created a double null mutant instead by designing guide RNAs to excise a large intergenic region between the tandem duplicate genes **(Fig. S1)**. We confirmed loss of Aldh2 protein by western blotting (**Fig. S1**). In keeping with our ALDH2i experiments, *aldh2-/-* mutants generated embryonic melanocytes, yet were defective in melanocyte regeneration from the McSC compartment **(Fig. 1D)**. We noticed that after multiple rounds of breeding, the melanocyte regeneration phenotype in our *aldh2-/-* mutants was lessened. This was coupled with transcriptional upregulation of other *aldh* enzyme family members suggesting some plasticity in *aldh* expression in regeneration and the possibility of genetic compensation by other Aldh enzymes (El-Brolosy et al. 2019) **(Fig. S1)**. To address this, we confirmed the *aldh2-/-* genetic mutant results in *aldh2.1 and aldh2.2* knockdown experiments with translation blocking morpholino oligonucleotides and once again showed that Aldh2 activity is specifically required in the McSC lineage, recapitulating the phenotype seen after Aldh2i **(Fig. S1, Fig. 1C)**. Finally, we found that the embryonic melanocytes in *aldh2-/-* mutants were defective for the dopaminergic camouflage response, a neuronally regulated innate behavior, reflecting the function for Aldh2 in dopamine metabolism (Yao et al. 2010). This phenotype recapitulates our previous data with Daidzin, another ALDH2i, and provides confidence that the *aldh2-/-* mutants are defective for Aldh2 activity (Zhou et al. 2012) **(Fig. S1)**.

Development • Accepted manuscript

Live imaging captures the McSC requirement for Aldh2 to generate progeny

To investigate whether Aldh2 activity impacts directly upon McSCs, we employed a *Tg(mitfa:GFP)* transgenic line that was previously shown to mark McSCs (Dooley et al. 2013; Brombin et al. 2022). Following ALDH2i treatment in regenerating embryos, we observed a significant reduction in GFP+ McSCs in the niche **(Fig. 2A)**. One interpretation of this result is that McSCs are depleted in the absence of Aldh2. Alternatively, McSCs may be present but expressing only low ~~(or no)~~ *mitfa:GFP* under conditions of ALDH2 inhibition.

In the earliest stages of embryonic development, McSCs that emerge from the neural crest maintain a neural crest identity at the niche, but lose this identity by day 3 (Brombin et al. 2022). Given our results in ALDH2i-treated regenerating embryos, we postulated that regenerative (activated) McSCs would re-express neural crest identity markers in addition to *mitfa*. To assess this hypothesis, we employed a double transgenic line *Tg(mitfa:GFP; crestin:mCherry)* in which *mCherry* is expressed from the promoter of the neural crest gene *crestin* (Kaufman et al. 2016; Brombin et al. 2022), and applied this to a second, independent regeneration assay. In this assay, the pro-drug MoTP kills differentiated embryonic melanocytes, and melanocytes are regenerated from the McSC compartment **(Fig. 1B)** (Yang and Johnson 2006). Following MoTP washout, McSCs expressed both mCherry and GFP in control animals **(Fig. 2B)**. McSCs were not detectable in non-regenerating embryos (without MoTP) **(Fig. 2C)**. In regenerating embryos, the intensity of GFP was heterogeneous between McSC clusters, but all McSCs expressed mCherry indicating that McSCs re-express a neural crest identity in regeneration **(Fig. 2B)**. Upon ALDH2i treatment, and as seen in **Fig. 2A**, we again observed a specific and strong reduction of GFP in McSCs, with mCherry+ McSCs still being clearly visible. Imaging niches at a higher magnification revealed a significant reduction in *mitfa:GFP* cells within McSC niches (**Fig. 2B**; **Fig.S2; Movie S1,2**). Thus, McSCs re-express a

Development • Accepted manuscript

neural crest marker during regeneration and require Aldh2 to increase expression of *mitfa* and generate melanoblasts.

Using live confocal imaging of McSCs to capture this process over time, we performed an MoTP regeneration assay and observed cells expressing high levels of *mitfa:GFP* emerging from McSCs and migrating dorsally in control embryos **(Fig. 2D; Movie S3)**. In contrast, the McSC niches in ALDH2i-treated embryos had little discernible cell movement, with very little *mitfa:GFP* expression **(Fig. 2D; Movie S4)**. Taken together, these data show that there are at least two distinct cell states within the regenerative McSC niche (*mitfa-low* and *mitfa-high*) and that Aldh2 is required for activated McSCs to increase *mitfa* expression and generate migratory progeny.

Aldh2, but not Adh5, is required for formaldehyde metabolism in McSCs

To elucidate the mechanism by which Aldh2 affects transitions between cell states in McSCs, we sought to identify its substrate. We reasoned that aldehyde substrates in melanocyte regeneration would be toxic if supplied in excess, and that toxicity would increase in *aldh2-/-* mutant embryos. Therefore, we screened known ALDH2 substrates for sensitivity in zebrafish development overall and specifically in the context of melanocyte regeneration **(Fig. 3A; Fig. S2)**. We found that *aldh2-/-* embryos were resistant to acetaldehyde and propionaldehyde, suggesting an unexpected plasticity in response to these aldehydes. *aldh2-/-* mutants were sensitized to 4-HNE, but this was not specific to the McSC lineage. Importantly, *aldh2-/-* embryos were sensitive to formaldehyde, and notably, low doses of exogenous formaldehyde (that had no other apparent effect on the fish) impaired melanocyte regeneration. This response was significantly stronger in *aldh2-/-* mutants compared to controls **(Fig. 3B, Fig. S2)**. These data indicate that formaldehyde, but not other aldehydes, is an important Aldh2 substrate in the McSC compartment.

Development • Accepted manuscript

Recent studies show that ALDH2 and ADH5 function together to clear endogenous formaldehyde during HSC differentiation to prevent immune depletion in mouse and induced pluripotent stem cells (iPSCs), as well as in patients with biallelic *ALDH2* and *ADH5* mutations (Dingler et al. 2020; Oka et al. 2020; Shen et al. 2020; Mu et al. 2021) **(Fig. 3C)**. Mice lacking both ALDH2 and ADH5 develop leukemia and have shorter lifespans, and despite active DNA repair, bone marrow-derived progenitors acquire a formaldehyde-associated mutation signature that resembles the human cancer mutation signatures associated with aging (Dingler et al. 2020). To address if Adh5 can function in melanocyte regeneration and compensate for Aldh2, we generated an *adh5-/-* mutant line by CRISPR-Cas9 **(Fig. 3D)**. We found that the *adh5-/-* mutant was highly sensitive to exogenous formaldehyde treatment, indicating that, like in mammals, formaldehyde is an Adh5 substrate in zebrafish **(Fig. 3E)**. However, *adh5* loss had no effect on melanocyte regeneration, and did not enhance the regeneration defects in *aldh2-/-* mutants or ALDH2i-treated embryos **(Fig. 3F, G)**. Thus, despite the shared formaldehyde substrate and conservation across species, Aldh2 has a unique function for formaldehyde metabolism in McSC differentiation, and Adh5 does not compensate for Aldh2 in this cell lineage.

scRNA-sequencing reveals Aldh2 is a metabolic gatekeeper for McSCs

Thus far, we had visually captured activated McSCs uncoupled from emerging progeny, and discovered a novel role for Aldh2 in this process in metabolizing endogenous formaldehyde in these cells. Next, we went on to investigate the transcriptional signatures of these cell populations by single cell RNA-sequencing (scRNA-seq) to ascertain how they might be affected by Aldh2 deficiency. To this end, we designed a scRNA-seq analysis of a MoTP melanocyte regeneration experiment in which double transgenic *mitfa:GFP; crestin:mCherry* embryos were treated with DMSO or CVT-10216, and then GFP+, mCherry+ and double+ cells

Development • Accepted manuscript

sorted together by FACS and processed for sequencing using the 10x protocol **(Fig. 4A)**. We identified 24 clusters of transcriptionally distinct cell populations by comparing the top 30 variably expressed genes, generating Uniform Manifold Approximation and Projection (UMAP)s featuring expression of known lineage-defining NC genes, and mapping the cluster identities from two recent zebrafish scRNA publications onto our data (Saunders et al. 2019; Farnsworth et al. 2020) **(Fig. 4B, C; Fig. S3; Tables S1, 2)**.

As *crestin:mCherry* is expressed in a wide range of neural crest-derived cell populations (Kaufman et al. 2016), we captured both pigment cell lineages and cells of the neural lineage. Clusters 7 and 11 expressed *crestin* and *mitfa,* with cluster 7 enriched for later stage melanoblast markers such as *dct*. Cells in clusters 2, 6 and 12 expressed *crestin*, but low *mitfa*, and mapping previously published scRNA-seq datasets onto this cluster reveals they contained a mix of pigment and neural cell identity markers, consistent with stem cell identity (Farnsworth et al. 2020; Brombin et al. 2022). Upon closer analyses of pigment cell clusters, we found that a subset of cluster 11 also shared these characteristics, suggesting that these are also McSCs (**Fig. S3**). *aldh2.2* and *aldh2.1* were expressed across multiple pigment cell clusters including McSCs and melanoblasts **(Fig. 4C)**. Relating the above cluster identities to our imaging analyses, we propose that the *crestin+ mitfa-low* McSCs are within clusters 2, 6 and 12 and that the *crestin+ mitfa-high* McSCs and progeny (and any remaining embryonic melanoblasts) are within clusters 7 and 11 **(Fig. 4D)**. The predicted cell cycle phase shows clusters 11 (*mitfa-high*) and 12 (*mitfa-low*) to be in S and G2/M, and may reflect the cycling McSCs we observe during regeneration **(Fig. 2D, 4D)**.

Next, we analyzed the dataset by drug treatment condition. Overall, we found that Aldh2 inhibition did not substantially change cell or cluster identity **(Fig. 4B)**. However, when comparing the numbers of cells within each cluster as a percentage of the total cell number per treatment condition, the proportions of cells within some clusters differed significantly **(Fig. 4E)**.

Development • Accepted manuscript

Specifically, we detected a higher proportion of *crestin+ mitfa-low* cells (clusters 2,6,12), and a lower proportion of *crestin+ mitfa-high* cells (cluster 7) after ALDH2i. This population shift is consistent with our imaging experiments, in which we detected fewer *mitfa:GFP* expressing cells at the McSC niche **(Fig. 2A, B, D)**, and is suggestive of a block in McSC differentiation.

To understand the physiological and mechanistic implications of the Aldh2-dependent *mitfa-high* to *mitfa-low* McSC transition, we performed differential expression analysis with the control dataset between *crestin+ mitfa-low* cells and *crestin+ mitfa-high* cells **(Table S3)**. *mitfa-high* cells (clusters 7,11) were enriched for pigmentation programs and melanoma-related terms, whereas *mitfa-low* cells (clusters 2,6,12) were enriched for essential metabolic pathways, including the 1C (THF) cycle, the TCA cycle, and *de novo* purine biosynthesis **(Fig. 4F)**, suggesting that regenerative McSCs have metabolic requirements distinct from those of melanoblasts.

Next, to understand why McSCs require Aldh2 activity to generate progeny, we performed differential expression analyses between controls and ALDH2i-treated cell populations **(Fig. 4G), Tables S4-6)**. Within the ALDH2i treated *crestin+ mitfa-low* cell population, *de novo* purine synthesis was again significantly upregulated **(Fig. 4G, H; Fig. S3)**, suggesting that McSCs “blocked” by ALDH2i are starved for purines. We found no ALDH2i-dependent change in *de novo* purine synthesis or glucose metabolism genes in cells from either clusters 7,11 or another pigment cell cluster requiring purine synthesis for pigmentation (cluster 9; iridophores) (Ng et al. 2009). Therefore, this pattern was specific to *crestin+ mitfa-low* cells and not a general effect of drug treatment. Taken together, these analyses support a mechanism in which regenerative McSCs require Aldh2 for metabolic rewiring in order to generate progeny.

Development • Accepted manuscript

Formate, the reaction product of Aldh2-dependent formaldehyde metabolism, promotes McSC transitions

One explanation for the Aldh2-deficient regeneration phenotype is that accumulation of endogenous formaldehyde causes McSC toxicity. However, we believe this to be unlikely given our experimental data: i) our observations while imaging over time showed no evidence of McSC disappearance, ii) following ALDH2i treatment, *crestin+ mitfa-low* McSCs were present in our scRNA-seq analysis, even at relatively higher numbers, and iii) the McSC block by ALDH2i treatment was reversible following washout **(Fig. S1)**. These findings led us to hypothesize that the reaction products of formaldehyde metabolism are required for timely McSCs differentiation but not for survival. To test this hypothesis, we performed a regeneration assay in CVT-10216 treated embryos in the presence or absence of formate and found that formate supplementation fully restored melanocyte regeneration **(Fig. 5A)**. At the cellular level, formate even fully rescued *crestin+ mitfa-high* McSCs at the niche site, while having no noticeable effect on *crestin:mCherry* expression **(Fig. 5B)**. These results indicate that formate, an Aldh2-dependent reaction product, promotes McSCs to transition from a *mitfa-low* to *mitfa-high* state to generate progeny.

McSCs require a functional 1C cycle

Formate is a carbon donor for the 1C cycle **(Fig. 5C)**. We found the McSC metabolic switch identified here was reminiscent of cell state transitions reported for naïve to primed murine stem cells that depend on 1C cycling and nucleotide biosynthesis (Chandrasekaran et al. 2017), as well as formate overflow mechanisms that induce a metabolic shift from low to high adenine nucleotide levels in human cancer cell lines and mouse cancer models (Oizel et al. 2020). Indeed, 1C metabolism, compartmentalized within different cell types and organs, is becoming more broadly recognized as a physiological process impacting on cell states and associated

Development • Accepted manuscript

with disease (Ducker and Rabinowitz 2017). Taken together, our data suggest that regenerative McSCs depend on 1C cycling to transition from a neural crest to a melanoblast cell state.

To test this hypothesis, we used the dihydrofolate reductase inhibitor methotrexate (Mtx) to inhibit 1C metabolism **(Fig. 5C-F)**. Mtx had no effect on the embryonic melanocyte lineage but its inhibitor function was easy to validate in zebrafish embryos; wild-type embryos treated with Mtx lack pigmentation in xanthophores and iridophores, both of which require functional 1C metabolism for pigment synthesis (Ng et al. 2009) **(Fig. 5D, S4)**. In the McSC lineage, we found that Mtx treatment caused melanocyte regeneration defects that were significantly exacerbated in *aldh2-/-* mutants **(Fig. 5E, F)**. These data indicate that zebrafish McSCs have metabolic requirements that require functional 1C metabolism.

Aldh2-dependent formaldehyde metabolism meets the demand of McSCs for purines

Given the upregulation of *de novo* purine metabolism genes in McSCs and their dependency on 1C metabolism, we next set out to examine purine nucleotide supplementation in regeneration. In the presence of ALDH2i, we found that exogenously provided purine nucleotides rescued the melanocyte regeneration defect in a dose-dependent manner **(Fig. 6A)**. This effect was not simply a consequence of providing embryos with an additional energy source in the form of ATP, because purine ribonucleosides were also capable of rescuing melanocyte regeneration **(Fig. 6B)**. However, pyrimidine supplementation did not rescue melanocyte regeneration, demonstrating that this effect does not reflect a general requirement for all nucleotides. Next, we explored the specificity of this rescue using confocal imaging, and found that purine, but not pyrimidine, supplementation selectively rescued *mitfa:GFP* expression at the McSC niche after ALDH2i treatment **(Fig. 6C, D)**. Hence, McSCs have a specific requirement for Aldh2 to generate progeny, and the end product of Aldh2 formaldehyde metabolism in McSCs is purine nucleotides **(Fig. 6E)**.

Development • Accepted manuscript

DISCUSSION

Understanding McSC responses to regenerative signals is central to the search for druggable targets for regenerative medicine and melanoma therapies (Patton et al. 2021). Here, we coupled single cell RNA sequencing with live imaging and chemical genetics in zebrafish McSCs to delineate how quiescent McSCs become activated and then transition to a proliferative state. By screening aldehyde substrates, we find melanocyte regeneration is sensitive to formaldehyde, is independent of *adh5*, and that the reaction product formate is sufficient to rescue Aldh2 deficiency. Thus, we identified an Aldh2-dependent mechanism exerting metabolic control of regeneration in McSCs, distinct from its aldehyde clearing mechanism. 8% of the world's population carry activity-reducing ALDH2 mutations and the underlying disease mechanism is considered to be elevated cellular toxicity. Thus, identification of an ALDH2-dependent gatekeeper mechanism for a regenerative stem cell response may have important ramifications for carriers of inactivating ALDH2 variants.

We find that regenerative McSCs re-activate a neural crest identity, which is reminiscent of the neural crest and melanocyte developmental states that become reactivated in melanoma disease progression (White et al. 2011; Shakhova et al. 2012; Konieczkowski et al. 2014; Kaufman et al. 2016; Rambow et al. 2018; Travnickova et al. 2019; Varum et al. 2019; Diener and Sommer 2020; Johansson et al. 2020; Marie et al. 2020). Although Dooley et al., (2013) detect *mitfa:GFP* expression at the niche throughout development, we consistently see a downregulation of *mitfa:GFP* expression in McSCs following establishment at the niche in non-regenerative conditions (**Figure 2;** Brombin et al., 2022); these differences may possibly be due to differences in imaging parameters and/or transgene expression. We use a combination of *aldh2* genetic mutants, morpholino knockdown studies and a highly selective ALDH2 inhibitor to reveal the function for Aldh2 in McSC metabolism (**Figure 1, Figure S1**). Given the selective expression of *aldh2* enzymes in the McSC (**Figure S1**) and the high selectivity of CVT-10216 for

Development • Accepted manuscript

ALDH2 over other ALDH enzymes, Aldh2 is likely the primary target of CVT-10216 in the McSC context, although additional studies will be required to understand if other ALDH enzymes are targets of CVT-10216 *in vivo*.

Notably, while all cells require nucleotides as fundamental building blocks, and for energy and signaling, the neural crest is especially sensitive to nucleotide depletion, which has direct metabolic consequences in rare disease and melanoma (Sporrij and Zon 2021). For instance, patients with Miller syndrome, a rare genetic neurocristopathy affecting face and limb development, have mutations in dihydroorotate dehydrogenase (DHODH), the rate-limiting enzyme for pyrimidine *de novo* biosynthesis (Ng et al. 2010; Sporrij and Zon 2021). In zebrafish, expression of a neural crest program defines melanoma initiation, and these cancers are sensitive to leflunomide, a DHODH inhibitor (White et al. 2011; Kaufman et al. 2016). Similarly, in mouse, a metabolic gene program driven by the transcription factor Yin Yang 1, a neural crest stem cell regulator, is essential for neural crest lineages, and its loss of function causes hypoplasia and prevents initiation of melanoma (Varum et al. 2019). In these contexts, nucleotide sensors may directly influence the transcriptional response, as we and others have shown for the neural crest and McSC differentiation (Johansson et al. 2020; Santoriello et al. 2020).

We were surprised to discover that regenerative McSCs have a select requirement for purine nucleotides (rather than pyrimidine nucleotides), findings that may point to purine nucleotide functions beyond transcription or DNA replication. For instance, purine nucleotides have an ancient function as neurotransmitters that activate purinergic receptors, and as such can regulate neural stem and progenitor cells, and melanocyte-keratinocyte communication in human skin (Ulrich et al. 2012; Lee et al. 2019). Hence, purine nucleotides could facilitate McSC communication with DRG niche cells (of which we know very little) and with peripheral nerves that are used as migratory routes for melanoblast progenitors (Budi et al. 2011; Dooley et al. 2013). Given that neural crest and McSCs programs re-emerge in melanoma, our findings may

Development • Accepted manuscript

be relevant to understanding the metabolic reprogramming in melanomas, such as the dependency on folate metabolism during melanoma metastasis (Piskounova et al. 2015; Fischer et al. 2018).

How stem cells generate progeny is a fundamental question in regenerative medicine. Here, we show that Aldh2-dependent formaldehyde metabolism underlies McSCs metabolic demand for purines to generate progeny. Formaldehyde is abundant in the blood (>40 µM) and can arise from demethylation reactions from histones and nucleic acids (Dingler et al. 2020; Mu et al. 2021). While ALDH2 is often thought of as a protective enzyme, we find no evidence of McSC toxicity in zebrafish with defective Aldh2 activity. Based on our data in **Fig. 3**, we suggest that an unknown endogenous formaldehyde source is active in melanocyte regeneration. Conceptually, our work identifies an unanticipated lineage-specific requirement for Aldh2 in the supply of essential metabolites in McSCs. This could mean that in individuals with inactivating mutations in ALDH2, both aldehyde cytotoxicity and depletion of aldehyde derived metabolites could result in the clinical disease features.

MATERIALS AND METHODS

Data and code availability

scRNA-seq experiment data will be made publicly available upon publication (GSE183868). Previously published sequencing data that was reanalyzed here are available from GEO: GSE131136 (Saunders et al. 2019), NCBI SRA: PRNJNA56410 (Farnsworth et al. 2020), and GEO: GSE178364 (Brombin et al. 2022).

Development • Accepted manuscript

Fish husbandry, fish lines

Zebrafish were maintained in accordance with UK Home Office regulations, UK Animals (Scientific Procedures) Act 1986, amended in 2013, and European Directive 2010/63/EU under project license 70/8000 and P8F7F7E52. All experiments were approved by the Home Office and AWERB (University of Edinburgh Ethics Committee). Fish stocks used were: wild-type AB, *mitfa*^{vc7} (Johnson et al. 2011; Zeng et al. 2015), *Tg(mitfa:GFP)* (Dooley et al. 2013), *Tg(crestin:mCherry)*(Kaufman et al. 2016), *aldh2-/-* (this study), and *adh5-/-* (this study). Combined transgenic and mutant lines were generated by crossing. Adult fish were maintained at ~28.5°C under 14:10 light-dark cycles. Embryos were kept at either 24°C, 28.5°C or 32°C and staged according to the reference table provided by Kimmel and colleagues (Kimmel et al. 1995).

Genotyping

Whole embryos or fin clips from adult fish were genotyped by resuspending tissue in DirectPCR® DNA-Tail solution (Viagen), and heating samples to 56°C for 2 hours, then 84°C for 20 minutes. Primers used for genotyping can be found in **Table S7**.

CRISPR-Cas9 mutant line generation

sgRNAs (**Table S7**) were synthesized using the EnGen® sgRNA Synthesis Kit, *S. pyogenes* (New England Biolabs) according to manufacturer's instructions. CRISPR-Cas9 knock-out lines were generated as previously described (Sorlien et al. 2018). Briefly, 200 ng/µl sgRNAs targeting exon 3 of *aldh2.1* (GCCAGAGATGCCTTTAAGCT) and exon 3 of *aldh2.2* (GCCAGAGATGCCTTTAAGCT) were co-injected with Cas9 mRNA into zebrafish embryos at the 1 cell stage. An allele was recovered which was the result of a large deletion between

Development • Accepted manuscript

aldh2.1 and *aldh2.2*, creating a gene fusion and single base-pair insertion at the fusion site. This introduced an adjacent frameshift mutation and premature stop codon.

200 ng/µl sgRNA targeting exon 3 of *adh5* (CTCAGTGGAAGTGACCCCGAG) was co-injected with recombinant 300 ng/µl Cas9 protein (SBI). These F0 fish were raised to adulthood, and outcrossed with WT fish to obtain progeny that were screened for presence of indels through PCR amplification of a 600bp region surrounding the target site, and digestion of the amplicon using T7 endonuclease (New England Biolabs). Outcrossed F1 fish that contained a 25bp deletion were isolated and raised to adulthood.

Morpholino injection

Standard control morpholinos and translation blocking morpholinos were sourced from Genetools LLC, based off previously published sequences for *aldh2.1* (ZDB-MRPHLNO-120517-2*)* and *aldh2.2* (ZDB-MRPHLNO-120517-3)(Ma et al. 2010). 2-6 ng of each morpholino was injected into sibling *mitfa*^{vc7} embryos at the 1-2 cell stage.

Imaging

Images of embryos immobilized with MS:222 and 1.5% LMP agarose were acquired using a 20X/0.75 lens on the multimodal Imaging Platform Dragonfly (Andor technologies, Belfast UK) equipped with 405, 445, 488, 514, 561, 640 and 680nm lasers built on a Nikon Eclipse Ti-E inverted microscope body with Perfect focus system (Nikon Instruments, Japan). Data were collected in Spinning Disk 40 µm pinhole mode on the Zyla 4.2 sCMOS camera using a Bin of 1 and no frame averaging using Andor Fusion acquisition software. Z stacks were collected using the Nikon TiE focus drive. Multiple positions were collected using a Sigma-Koki Stage (Nikon Instruments Japan). Data were visualized and analyzed using Imaris (Oxford Instruments, v. 9.7.0) or Image J Fiji software (v. 1.53c).

Development • Accepted manuscript

Whole zebrafish embryos fixed in 4% PFA/PBST were imaged with a Leica MZFLIII fluorescence stereo microscope with a 1x objective fitted with a Qimaging Retiga Exi CCD camera (Qimaging, Surrey, BC, Canada). Image capture was performed using Micromanager (Version 1.4).

To quantify the area of *GFP* or *mCherry*-expressing cells within niches, homozygous *Tg(mitfa:GFP)* fish were outcrossed with non-fluorescent or *Tg(crestin:mCherry)* fish to obtain embryos with similar levels of transgene expression. The McSC compartment was imaged at the same magnification, within the same anatomical area, and with consistent laser power and other imaging settings between individual samples and biological replicates. In Fiji, a maximum projection Z-stack of images was cropped to only include McSC compartment cells (typically containing 6-7 compartments per image) and converted to a binary image. Consistent threshold settings were applied, and the total GFP+ area measured in pixels^2 and divided by the number of somites visible in the field of view.

Melanocyte regeneration assays

If using the *mitfa*^{vc7} regeneration model line, embryos were kept in a 32°C incubator from 0-72hpf to repress the developmental melanocyte lineage. Embryos were then moved to a 24°C incubator to allow regeneration over a period of 48 hours. When using chemical methods for regeneration, 150 μM 4-(4-Morpholinobutylthio)phenol (MoTP) (Sigma-Aldrich) was added to embryos kept at 28.5°C from 24hpf onwards. MoTP was washed out to allow regeneration between 72 and 120 hpf. After fixation, embryos were imaged and melanocytes counted using the Image J CellCounter plugin within a consistent dorsal area outlined in **Fig. 1C**. Embryos were imaged dorsally, and only in-focus dorsal surface melanocytes counted. For the anterior and posterior bounds, anatomical landmarks used include the anterior-most portion of the head, but excluding any in-focus melanocytes around the mouth. Posteriorly, we counted until the

Development • Accepted manuscript

point at which the yolk 'pinches off' as it meets the tail. This gave a uniform and wide area within which to count melanocytes consistently and gauge differences in number between drug treatments.

Camouflage response assays

The camouflage response assay was performed as described previously (Zhou et al. 2012). 5 dpf wild type or *aldh2-/-* mutant embryos were placed in darkness for 15 minutes to standardize their light exposure. These embryos were split into cohorts which were either placed under a lamp or kept in the dark for 1.5 hours. The embryos were then moved to the opposite light condition for a further 45 minutes, during which time melanin dispersed or contracted depending on light exposure. This was repeated once or twice more when assessing the embryos ability to learn to adapt to changing light conditions. Afterwards, embryos were then briefly anaesthetized in MS-222 and fixed in 4% PFA. Embryos were imaged dorsally at a fixed magnification. Melanin coverage was measured with Image J Fiji, by outlining a predetermined region of the head, converting the image to an 8-bit binary image with a uniform threshold, and then measuring the area of black pixels.

Small molecule inhibitor and rescue experiments

Unless otherwise stated, 10 μM CVT-10216 (Sigma-Aldrich) or equimolar Dimethyl Sulphoxide DMSO (Sigma-Aldrich) was added to embryos at 24hpf after manual or pronase-assisted (Merck) dechorionation and refreshed every 24 hours. Embryos were arrayed in 6-well tissue culture plates with 10-15 embryos per well. For formate supplementation assays, 25 μM sodium formate (Merck) was added. For nucleotide supplementation assays, 400 μM of AMP, UMP, GMP, IMP or TMP (Merck) were added to embryos, or 200 μM of dA, dG, dU or T (Merck). 4-

Development • Accepted manuscript

HNE (range of concentrations in ethanol) (Calbiochem) and Mtx (Merck) (range of concentrations in DMSO) were added at 24hpf and refreshed every 24 hours.

Aldehyde treatments

Stock solutions of fresh acetaldehyde (Merck) and formaldehyde (VWR International) were made in a fume hood just before use. Various aldehyde concentrations were added to embryos kept in screw cap centrifuge tubes to limit aldehyde evaporation, and embryos scored for survival after 48 hours.

RNA extraction and RT-qPCR

Samples to be processed for RT-qPCR were collected at the required stage and frozen on dry ice. RNA was extracted from frozen tissues with the Qiagen RNeasy Mini kit according to manufacturer's instructions. RNA was quantified and quality checked using a Nanodrop 2000c (Thermo Scientific). 500 µg of RNA was used as input for Reverse Transcription using Superscript™ III reverse transcriptase (Invitrogen) and an Oligo$(DT)_{15}$ primer (Promega). RT-qPCR was performed with Sybr Green® Lightcycler Green I Master mix (Roche), using a Lightcycler 480 instrument and associated software. RT-qPCR primers (**Table S7**) were designed using Primer 3 Plus software to amplify ~120bp regions over exon-intron junctions. In the case of using RT-qPCR to detect *aldh2-/-* mutant transcripts, these regions were picked to be either in a predicted region of *aldh2.1* still present after the fusion event (Primer site 1, exon 5 of *aldh2.1*, **Fig. S1**), or within a region of aldh2.2 predicted to disappear after excision of the intergenic region between *aldh2.1* and *aldh2.2* (Primer site 2, exon 13 of *aldh2.2*). *β-actin* was used as a housekeeping control. Gene expression fold changes were found using the delta-delta ct method.

Development • Accepted manuscript

Western blotting

50 WT or *aldh2-/-* mutant embryos were processed for western blot analysis by deyolking and then homogenizing in RIPA buffer containing cOmplete™ Protease Inhibitor cocktail (Merck). After centrifugation, the protein content of the supernatant was measured with a BCA Protein Assay Kit (Thermo Fisher), and ~10µg of protein loaded onto a Mini-PROTEAN TGX Precast Gel (Biorad). Nitrocellulose membranes (Biorad) were blocked with 5% BSA in PBS-Tween and incubated with either anti-ALDH2 antibody (1:2000, 15310-0-1-AP, Proteintech) or anti-Histone H3 antibody (1:1000, ab10799, Abcam) overnight and then IRDye® 800CW Donkey anti-Rabbit IgG secondary antibody (1:10000, RRID: AB_621848, Licor) or IRDye® 680RD Donkey anti-Mouse IgG secondary antibody (1:10000, RRID: AB_10953628, Licor) respectively were incubated for 1 hour. Blots were imaged using the Odyssey Infrared Imaging System and associated software (Licor).

Single cell sequencing experimental setup and sequencing

24hpf *Tg(mitfa:GFP; crestin:mCherry)* were divided into groups of ~500 embryos and treated with MoTP, and co-treated with either 10 µM CVT-10216 or equimolar DMSO. At 64hpf, MoTP was washed out, and embryos left to regenerate for 8 hours. Embryos were anaesthetized in MS-222 and trunks dissected, and a cell suspension of each treatment condition obtained as previously described (Manoli and Driever 2012). Samples were sorted on a FACSAria2 SORP instrument (BD Biosciences UK) as previously described (Brombin et al. 2022) but stage-matched non-fluorescent AB embryos also treated with MoTP used as a control to enable gating of *mCherry* and *GFP* fluorescence. 10,000 GFP+, mCherry+ or double+ cells per treatment condition were sorted together into 100 µl of 0.04% BSA/PBS and processed for the 10x protocol. Single cell libraries were prepared using the Chromium Single Cell 3' GEM, Library & Gel Bead Kit v3 (10x Genomics).

Development • Accepted manuscript

The samples were sequenced on a Nextseq 2000 using a P2 flow cell on a 100 cycle run. ~2.97M reads passed quality filters for CVT-10216 treated, and ~1.87M reads for DMSO-treated, however due to the greater number of cells processed in the CVT-10216 sample, the mean reads per cell were fairly equal (37,405-CVT vs 34,832-DMSO).

Bioinformatics analyses

Aldh2.2 expression within developmental melanocytes was visualized using the recent Brombin et al. GEO #: GSE178364 scRNA-seq dataset (Brombin et al. 2022).

For this study, FASTQ files were generated using CellRanger (v.3.1.0, 10x Genomics) mkfastq function with default settings and -qc parameter and aligned to the zebrafish STAR genome index using gene annotations from Ensembl GRCz11 release 94 with manually annotated entries for *GFP* and *mCherry*. Libraries were aggregated (CellRanger aggr pipeline) to generate a gene-barcode matrix. Gene matrices (13360 total, DMSO-5,394, CVT-7966), barcodes and features were uploaded to R (v. 4.0.5) and standard quality control filtering performed as previously described, to yield 4488 DMSO and 6795 CVT cells (Brombin et al. 2022). The dimensionality of the combined dataset was visualized with Elbow and JackStraw plots before running linear dimensional reduction. Louvain clustering was then performed using the FindNeighbors and FindClusters functions (dims=50, resolution=0.5) in Seurat (v. 4.0.3) (Hao et al. 2021). Data were projected onto 2D spaces using the same dimensions, using Uniform Manifold Approximation and Projection (UMAP). Cluster-specific genes were identified using Seurat as previously described (**Table S1,2**) (Brombin et al. 2022).

Cluster calling was performed as previously described (Brombin et al. 2022) and by making unbiased pairwise comparisons based on gene overdispersion against published datasets GEO #: GSE131136 (Saunders et al. 2019) and NCBI SRA #: PRNJNA56410 (Farnsworth et al. 2020) and between the datasets presented in this paper as previously

Development • Accepted manuscript

described (Brombin et al. 2022). Plots were generated either using Seurat or ggplot2 (v.3.3.5) (Wickham 2016). Prediction of cell cycle phase was performed with Seurat, using canonical cell cycle markers described in (Tirosh et al. 2016).

For DE analyses, scRNA-seq data were first corrected for zero-inflated counts by using the ZINB-WaVE package (v. 1.12.0) with default parameters (Risso et al. 2019). Then, the DEseq2 package (v. 1.30.1) (Love et al. 2014) was used to generate genelists of significantly (p.adj < 0.05) upregulated and downregulated genes (raw data in **Tables S3-6**). Pathway analyses were performed as previously described (Travnickova et al. 2019). GSEA analysis was performed using GSEA software (v. 4.1.0) with genelists generated through DeSeq2, using the "RunGSEAPreranked" function.

For phylogenetic analyses, FASTA sequences for human and zebrafish ALDH proteins were aligned with the online T-Coffee multiple sequence alignment, and the phylogeny feature used to construct a tree.

Statistics

Statistical details of experiments and n numbers can be found in figure legends. Statistics and plots were generated using GraphPad Prism 7 (v. 7.0e) and R.

ACKNOWLEDGEMENTS

We are grateful to Cameron Wyatt and the IGC Zebrafish Facility for zebrafish management and husbandry, Elisabeth Freyer and the IGC FACS/10x facility, Ann Wheeler and the IGC Imaging Facility for supporting the imaging experiments, Richard Clarke at the Genetics Core ECRF for sequencing, Yuting Lu for sharing RT-qPCR primers, Jana Travnickova, Neil Robertson and Tamir Chandra for bioinformatics support, and Christina Lilliehook for editorial support.

Development • Accepted manuscript

COMPETING INTERESTS STATEMENT

The authors declare no competing interests.

FUNDING

JHP is supported by US National Institutes of Health grants R01 OD011116 and R24 OD018555. EEP is funded by MRC HGU Program (MC_UU_00007/9), the European Research Council (ZF-MEL-CHEMBIO-648489), and Melanoma Research Alliance (687306).

Author Contributions:

Conceptualization: EEP, HB; Methodology: HB; Software: HB; Validation: HB; Formal analysis: HB, AB; Investigation: HB, AB, SP, JHP; Resources: SP, JHP, EEP; Writing original draft: EEP, HB; Writing review and editing: HB, AB, JHP, EEP; Visualization: HB, EEP; Supervision: JHP, EEP; Funding acquisition: JHP, EEP.

REFERENCES

Adameyko I, Lallemend F, Aquino JB, Pereira JA, Topilko P, Muller T, Fritz N, Beljajeva A, Mochii M, Liste I et al. 2009. Schwann cell precursors from nerve innervation are a cellular origin of melanocytes in skin. *Cell* **139**: 366-379.

Bae S, Chon J, Field MS, Stover PJ. 2017. Alcohol Dehydrogenase 5 Is a Source of Formate for De Novo Purine Biosynthesis in HepG2 Cells. *J Nutr* **147**: 499-505.

Baggiolini A, Callahan SJ, Montal E, Weiss JM, Trieu T, Tagore MM, Tischfield SE, Walsh RM, Suresh S, Fan Y et al. 2021. Developmental chromatin programs determine oncogenic competence in melanoma. *Science* **373**: eabc1048.

Brombin A, Simpson DJ, Travnickova J, Brunsdon H, Zeng Z, Lu Y, Young AIJ, Chandra T, Patton EE. 2022. Tfap2b specifies an embryonic melanocyte stem cell that retains adult multifate potential. *Cell Rep* **38**: 110234.

Development • Accepted manuscript

Brooks PJ, Enoch MA, Goldman D, Li TK, Yokoyama A. 2009. The alcohol flushing response: an unrecognized risk factor for esophageal cancer from alcohol consumption. *PLoS Med* **6**: e50.

Budi EH, Patterson LB, Parichy DM. 2008. Embryonic requirements for ErbB signaling in neural crest development and adult pigment pattern formation. *Development* **135**: 2603-2614.

-. 2011. Post-embryonic nerve-associated precursors to adult pigment cells: genetic requirements and dynamics of morphogenesis and differentiation. *PLoS Genet* **7**: e1002044.

Burgos-Barragan G, Wit N, Meiser J, Dingler FA, Pietzke M, Mulderrig L, Pontel LB, Rosado IV, Brewer TF, Cordell RL et al. 2017. Mammals divert endogenous genotoxic formaldehyde into one-carbon metabolism. *Nature* **548**: 549-554.

Chandrasekaran S, Zhang J, Sun Z, Zhang L, Ross CA, Huang YC, Asara JM, Li H, Daley GQ, Collins JJ. 2017. Comprehensive Mapping of Pluripotent Stem Cell Metabolism Using Dynamic Genome-Scale Network Modeling. *Cell Rep* **21**: 2965-2977.

Chang JS, Hsiao JR, Chen CH. 2017. ALDH2 polymorphism and alcohol-related cancers in Asians: a public health perspective. *J Biomed Sci* **24**: 19.

Chen CH, Ferreira JC, Gross ER, Mochly-Rosen D. 2014. Targeting aldehyde dehydrogenase 2: new therapeutic opportunities. *Physiol Rev* **94**: 1-34.

Chen CH, Ferreira JCB, Joshi AU, Stevens MC, Li SJ, Hsu JH, Maclean R, Ferreira ND, Cervantes PR, Martinez DD et al. 2020. Novel and prevalent non-East Asian ALDH2 variants; Implications for global susceptibility to aldehydes' toxicity. *EBioMedicine* **55**: 102753.

Chou WC, Takeo M, Rabbani P, Hu H, Lee W, Chung YR, Carucci J, Overbeek P, Ito M. 2013. Direct migration of follicular melanocyte stem cells to the epidermis after wounding or UVB irradiation is dependent on Mc1r signaling. *Nat Med* **19**: 924-929.

Diener J, Sommer L. 2020. Reemergence of neural crest stem cell-like states in melanoma during disease progression and treatment. *Stem Cells Transl Med*.

Dingler FA, Wang M, Mu A, Millington CL, Oberbeck N, Watcham S, Pontel LB, Kamimae-Lanning AN, Langevin F, Nadler C et al. 2020. Two Aldehyde Clearance Systems Are Essential to Prevent Lethal Formaldehyde Accumulation in Mice and Humans. *Mol Cell* **80**: 996-1012 e1019.

Development • Accepted manuscript

Dooley CM, Mongera A, Walderich B, Nusslein-Volhard C. 2013. On the embryonic origin of adult melanophores: the role of ErbB and Kit signalling in establishing melanophore stem cells in zebrafish. *Development* **140**: 1003-1013.

Ducker GS, Rabinowitz JD. 2017. One-Carbon Metabolism in Health and Disease. *Cell Metab* **25**: 27-42.

El-Brolosy MA, Kontarakis Z, Rossi A, Kuenne C, Gunther S, Fukuda N, Kikhi K, Boezio GLM, Takacs CM, Lai SL et al. 2019. Genetic compensation triggered by mutant mRNA degradation. *Nature* **568**: 193-197.

Farnsworth DR, Saunders LM, Miller AC. 2020. A single-cell transcriptome atlas for zebrafish development. *Dev Biol* **459**: 100-108.

Fischer GM, Vashisht Gopal YN, McQuade JL, Peng W, DeBerardinis RJ, Davies MA. 2018. Metabolic strategies of melanoma cells: Mechanisms, interactions with the tumor microenvironment, and therapeutic implications. *Pigment Cell Melanoma Res* **31**: 11-30.

Garaycoechea JI, Crossan GP, Langevin F, Daly M, Arends MJ, Patel KJ. 2012. Genotoxic consequences of endogenous aldehydes on mouse haematopoietic stem cell function. *Nature* **489**: 571-575.

Garaycoechea JI, Crossan GP, Langevin F, Mulderrig L, Louzada S, Yang F, Guilbaud G, Park N, Roerink S, Nik-Zainal S et al. 2018. Alcohol and endogenous aldehydes damage chromosomes and mutate stem cells. *Nature* **553**: 171-177.

Hao Y, Hao S, Andersen-Nissen E, Mauck WM, 3rd, Zheng S, Butler A, Lee MJ, Wilk AJ, Darby C, Zager M et al. 2021. Integrated analysis of multimodal single-cell data. *Cell* **184**: 3573-3587 e3529.

Harada S, Agarwal DP, Goedde HW. 1981. Aldehyde dehydrogenase deficiency as cause of facial flushing reaction to alcohol in Japanese. *Lancet* **2**: 982.

Hiura Y, Tabara Y, Kokubo Y, Okamura T, Miki T, Tomoike H, Iwai N. 2010. A genome-wide association study of hypertension-related phenotypes in a Japanese population. *Circ J* **74**: 2353-2359.

Hodskinson MR, Bolner A, Sato K, Kamimae-Lanning AN, Rooijers K, Witte M, Mahesh M, Silhan J, Petek M, Williams DM et al. 2020. Alcohol-derived DNA crosslinks are repaired by two distinct mechanisms. *Nature* **579**: 603-608.

Development • Accepted manuscript

Hultman KA, Budi EH, Teasley DC, Gottlieb AY, Parichy DM, Johnson SL. 2009. Defects in ErbB-dependent establishment of adult melanocyte stem cells reveal independent origins for embryonic and regeneration melanocytes. *PLoS Genet* **5**: e1000544.

Irion U, Nusslein-Volhard C. 2019. The identification of genes involved in the evolution of color patterns in fish. *Curr Opin Genet Dev* **57**: 31-38.

Jacobson MK, Bernofsky C. 1974. Mitochondrial acetaldehyde dehydrogenase from Saccharomyces cerevisiae. *Biochim Biophys Acta* **350**: 277-291.

Johansson JA, Marie KL, Lu Y, Brombin A, Santoriello C, Zeng Z, Zich J, Gautier P, von Kriegsheim A, Brunsdon H et al. 2020. PRL3-DDX21 Transcriptional Control of Endolysosomal Genes Restricts Melanocyte Stem Cell Differentiation. *Dev Cell* **54**: 317-332 e319.

Johnson SL, Nguyen AN, Lister JA. 2011. mitfa is required at multiple stages of melanocyte differentiation but not to establish the melanocyte stem cell. *Dev Biol* **350**: 405-413.

Jung M, Smogorzewska A. 2021. Endogenous formaldehyde destroys blood stem cells. *Blood* **137**: 1988-1990.

Kaufman CK, Mosimann C, Fan ZP, Yang S, Thomas AJ, Ablain J, Tan JL, Fogley RD, van Rooijen E, Hagedorn EJ et al. 2016. A zebrafish melanoma model reveals emergence of neural crest identity during melanoma initiation. *Science* **351**: aad2197.

Kelsh RN, Barsh GS. 2011. A nervous origin for fish stripes. *PLoS Genet* **7**: e1002081.

Kelsh RN, Brand M, Jiang YJ, Heisenberg CP, Lin S, Haffter P, Odenthal J, Mullins MC, van Eeden FJ, Furutani-Seiki M et al. 1996. Zebrafish pigmentation mutations and the processes of neural crest development. *Development* **123**: 369-389.

Kimmel CB, Ballard WW, Kimmel SR, Ullmann B, Schilling TF. 1995. Stages of embryonic development of the zebrafish. *Dev Dyn* **203**: 253-310.

Konieczkowski DJ, Johannessen CM, Abudayyeh O, Kim JW, Cooper ZA, Piris A, Frederick DT, Barzily-Rokni M, Straussman R, Haq R et al. 2014. A melanoma cell state distinction influences sensitivity to MAPK pathway inhibitors. *Cancer Discov* **4**: 816-827.

Langevin F, Crossan GP, Rosado IV, Arends MJ, Patel KJ. 2011. Fancd2 counteracts the toxic effects of naturally produced aldehydes in mice. *Nature* **475**: 53-58.

Development • Accepted manuscript

Lee EJ, Kim JY, Ahn Y, Lee BM, Heo Y, Hwang S, Lee SH, Lee J, Chung G, Oh SH. 2019. Critical Role of ATP-P2X7 Axis in UV-Induced Melanogenesis. *J Invest Dermatol* **139**: 1554-1563 e1556.

Love MI, Huber W, Anders S. 2014. Moderated estimation of fold change and dispersion for RNA-seq data with DESeq2. *Genome Biol* **15**: 550.

Ma AC, Chung MI, Liang R, Leung AY. 2010. A DEAB-sensitive aldehyde dehydrogenase regulates hematopoietic stem and progenitor cells development during primitive hematopoiesis in zebrafish embryos. *Leukemia* **24**: 2090-2099.

Manoli M, Driever W. 2012. Fluorescence-activated cell sorting (FACS) of fluorescently tagged cells from zebrafish larvae for RNA isolation. *Cold Spring Harb Protoc* **2012**.

Marcato P, Dean CA, Giacomantonio CA, Lee PW. 2011. Aldehyde dehydrogenase: its role as a cancer stem cell marker comes down to the specific isoform. *Cell Cycle* **10**: 1378-1384.

Marie KL, Sassano A, Yang HH, Michalowski AM, Michael HT, Guo T, Tsai YC, Weissman AM, Lee MP, Jenkins LM et al. 2020. Melanoblast transcriptome analysis reveals pathways promoting melanoma metastasis. *Nat Commun* **11**: 333.

Masaoka H, Ito H, Soga N, Hosono S, Oze I, Watanabe M, Tanaka H, Yokomizo A, Hayashi N, Eto M et al. 2016. Aldehyde dehydrogenase 2 (ALDH2) and alcohol dehydrogenase 1B (ADH1B) polymorphisms exacerbate bladder cancer risk associated with alcohol drinking: gene-environment interaction. *Carcinogenesis* **37**: 583-588.

Matsuo K, Oze I, Hosono S, Ito H, Watanabe M, Ishioka K, Ito S, Tajika M, Yatabe Y, Niwa Y et al. 2013. The aldehyde dehydrogenase 2 (ALDH2) Glu504Lys polymorphism interacts with alcohol drinking in the risk of stomach cancer. *Carcinogenesis* **34**: 1510-1515.

Mort RL, Jackson IJ, Patton EE. 2015. The melanocyte lineage in development and disease. *Development* **142**: 620-632.

Mu A, Hira A, Niwa A, Osawa M, Yoshida K, Mori M, Okamoto Y, Inoue K, Kondo K, Kanemaki MT et al. 2021. Analysis of disease model iPSCs derived from patients with a novel Fanconi anemia-like IBMFS ADH5/ALDH2 deficiency. *Blood* **137**: 2021-2032.

Nakamura J, Holley DW, Kawamoto T, Bultman SJ. 2020. The failure of two major formaldehyde catabolism enzymes (ADH5 and ALDH2) leads to partial synthetic lethality in C57BL/6 mice. *Genes Environ* **42**: 21.

Development • Accepted manuscript

Ng A, Uribe RA, Yieh L, Nuckels R, Gross JM. 2009. Zebrafish mutations in gart and paics identify crucial roles for de novo purine synthesis in vertebrate pigmentation and ocular development. *Development* **136**: 2601-2611.

Ng SB, Buckingham KJ, Lee C, Bigham AW, Tabor HK, Dent KM, Huff CD, Shannon PT, Jabs EW, Nickerson DA et al. 2010. Exome sequencing identifies the cause of a mendelian disorder. *Nat Genet* **42**: 30-35.

Nishimura EK, Granter SR, Fisher DE. 2005. Mechanisms of hair graying: incomplete melanocyte stem cell maintenance in the niche. *Science* **307**: 720-724.

O'Brien PJ, Siraki AG, Shangari N. 2005. Aldehyde sources, metabolism, molecular toxicity mechanisms, and possible effects on human health. *Crit Rev Toxicol* **35**: 609-662.

Oizel K, Tait-Mulder J, Fernandez-de-Cossio-Diaz J, Pietzke M, Brunton H, Lilla S, Dhayade S, Athineos D, Blanco GR, Sumpton D et al. 2020. Formate induces a metabolic switch in nucleotide and energy metabolism. *Cell Death Dis* **11**: 310.

Oka Y, Hamada M, Nakazawa Y, Muramatsu H, Okuno Y, Higasa K, Shimada M, Takeshima H, Hanada K, Hirano T et al. 2020. Digenic mutations in ALDH2 and ADH5 impair formaldehyde clearance and cause a multisystem disorder, AMeD syndrome. *Sci Adv* **6**.

Owen JP, Kelsh RN, Yates CA. 2020. A quantitative modelling approach to zebrafish pigment pattern formation. *Elife* **9**.

Patton EE, Mueller KL, Adams DJ, Anandasabapathy N, Aplin AE, Bertolotto C, Bosenberg M, Ceol CJ, Burd CE, Chi P et al. 2021. Melanoma models for the next generation of therapies. *Cancer Cell* **39**: 610-631.

Piskounova E, Agathocleous M, Murphy MM, Hu Z, Huddlestun SE, Zhao Z, Leitch AM, Johnson TM, DeBerardinis RJ, Morrison SJ. 2015. Oxidative stress inhibits distant metastasis by human melanoma cells. *Nature* **527**: 186-191.

Pontel LB, Rosado IV, Burgos-Barragan G, Garaycoechea JI, Yu R, Arends MJ, Chandrasekaran G, Broecker V, Wei W, Liu L et al. 2015. Endogenous Formaldehyde Is a Hematopoietic Stem Cell Genotoxin and Metabolic Carcinogen. *Mol Cell* **60**: 177-188.

Rambow F, Rogiers A, Marin-Bejar O, Aibar S, Femel J, Dewaele M, Karras P, Brown D, Chang YH, Debiec-Rychter M et al. 2018. Toward Minimal Residual Disease-Directed Therapy in Melanoma. *Cell* **174**: 843-855 e819.

Development • Accepted manuscript

Risso D, Perraudeau F, Gribkova S, Dudoit S, Vert JP. 2019. Publisher Correction: A general and flexible method for signal extraction from single-cell RNA-seq data. *Nat Commun* **10**: 646.

Rosado IV, Langevin F, Crossan GP, Takata M, Patel KJ. 2011. Formaldehyde catabolism is essential in cells deficient for the Fanconi anemia DNA-repair pathway. *Nat Struct Mol Biol* **18**: 1432-1434.

Santoriello C, Sporrij A, Yang S, Flynn RA, Henriques T, Dorjsuren B, Custo Greig E, McCall W, Stanhope ME, Fazio M et al. 2020. RNA helicase DDX21 mediates nucleotide stress responses in neural crest and melanoma cells. *Nat Cell Biol* **22**: 372-379.

Saunders LM, Mishra AK, Aman AJ, Lewis VM, Toomey MB, Packer JS, Qiu X, McFaline-Figueroa JL, Corbo JC, Trapnell C et al. 2019. Thyroid hormone regulates distinct paths to maturation in pigment cell lineages. *Elife* **8**.

Shakhova O, Zingg D, Schaefer SM, Hari L, Civenni G, Blunschi J, Claudinot S, Okoniewski M, Beermann F, Mihic-Probst D et al. 2012. Sox10 promotes the formation and maintenance of giant congenital naevi and melanoma. *Nat Cell Biol* **14**: 882-890.

Shen X, Wang R, Kim MJ, Hu Q, Hsu CC, Yao J, Klages-Mundt N, Tian Y, Lynn E, Brewer TF et al. 2020. A Surge of DNA Damage Links Transcriptional Reprogramming and Hematopoietic Deficit in Fanconi Anemia. *Mol Cell* **80**: 1013-1024 e1016.

Singh AP, Dinwiddie A, Mahalwar P, Schach U, Linker C, Irion U, Nusslein-Volhard C. 2016. Pigment Cell Progenitors in Zebrafish Remain Multipotent through Metamorphosis. *Dev Cell* **38**: 316-330.

Sorlien EL, Witucki MA, Ogas J. 2018. Efficient Production and Identification of CRISPR/Cas9-generated Gene Knockouts in the Model System Danio rerio. *J Vis Exp*.

Sporrij A, Zon LI. 2021. Nucleotide stress responses in neural crest cell fate and melanoma. *Cell Cycle* **20**: 1455-1467.

Takeuchi F, Yokota M, Yamamoto K, Nakashima E, Katsuya T, Asano H, Isono M, Nabika T, Sugiyama T, Fujioka A et al. 2012. Genome-wide association study of coronary artery disease in the Japanese. *Eur J Hum Genet* **20**: 333-340.

Tirosh I, Venteicher AS, Hebert C, Escalante LE, Patel AP, Yizhak K, Fisher JM, Rodman C, Mount C, Filbin MG et al. 2016. Single-cell RNA-seq supports a developmental hierarchy in human oligodendroglioma. *Nature* **539**: 309-313.

Development • Accepted manuscript

Travnickova J, Patton EE. 2021. Deciphering Melanoma Cell States and Plasticity with Zebrafish Models. *J Invest Dermatol* **141**: 1389-1394.

Travnickova J, Wojciechowska S, Khamseh A, Gautier P, Brown DV, Lefevre T, Brombin A, Ewing A, Capper A, Spitzer M et al. 2019. Zebrafish MITF-Low Melanoma Subtype Models Reveal Transcriptional Subclusters and MITF-Independent Residual Disease. *Cancer Res* **79**: 5769-5784.

Ulrich H, Abbracchio MP, Burnstock G. 2012. Extrinsic purinergic regulation of neural stem/progenitor cells: implications for CNS development and repair. *Stem Cell Rev Rep* **8**: 755-767.

Varum S, Baggiolini A, Zurkirchen L, Atak ZK, Cantu C, Marzorati E, Bossart R, Wouters J, Hausel J, Tuncer E et al. 2019. Yin Yang 1 Orchestrates a Metabolic Program Required for Both Neural Crest Development and Melanoma Formation. *Cell Stem Cell* **24**: 637-653 e639.

White RM, Cech J, Ratanasirintrawoot S, Lin CY, Rahl PB, Burke CJ, Langdon E, Tomlinson ML, Mosher J, Kaufman C et al. 2011. DHODH modulates transcriptional elongation in the neural crest and melanoma. *Nature* **471**: 518-522.

Wickham H. 2016. *ggplot2: Elegant Graphics for Data Analysis*. Springer-Verlag New York.

Yang CT, Johnson SL. 2006. Small molecule-induced ablation and subsequent regeneration of larval zebrafish melanocytes. *Development* **133**: 3563-3573.

Yao L, Fan P, Arolfo M, Jiang Z, Olive MF, Zablocki J, Sun HL, Chu N, Lee J, Kim HY et al. 2010. Inhibition of aldehyde dehydrogenase-2 suppresses cocaine seeking by generating THP, a cocaine use-dependent inhibitor of dopamine synthesis. *Nat Med* **16**: 1024-1028.

Zeng Z, Johnson SL, Lister JA, Patton EE. 2015. Temperature-sensitive splicing of mitfa by an intron mutation in zebrafish. *Pigment Cell Melanoma Res* **28**: 229-232.

Zhou L, Ishizaki H, Spitzer M, Taylor KL, Temperley ND, Johnson SL, Brear P, Gautier P, Zeng Z, Mitchell A et al. 2012. ALDH2 mediates 5-nitrofuran activity in multiple species. *Chem Biol* **19**: 883-892.

Development • Accepted manuscript

Figures

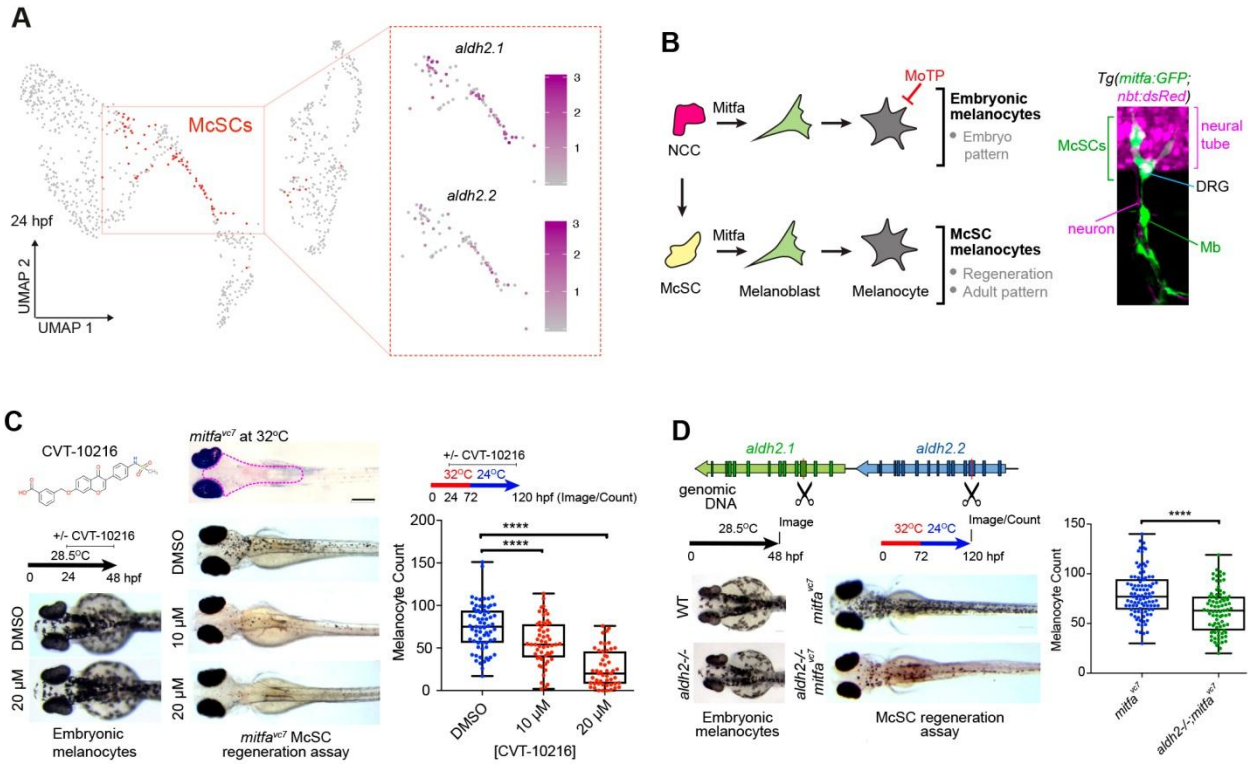

Figure 1: **Lineage-specific requirement for Aldh2 in melanocyte regeneration**

A. UMAP of scRNA-seq data derived from 24hpf embryos (Brombin et al, 2022) with McSCs in red. Feature plots of these isolated McSCs showing $\log_2$ expression of *aldh2* paralogs with color change from grey (negative) to purple.

B. Schematic of the melanocyte lineages in zebrafish development with confocal Z-stacks depicting McSCs expressing *mitfa:GFP* located at the dorsal root ganglia (DRG) and melanoblasts (Mb) on the motor neurons. Neural tube and DRG are marked by *nbt:dsRed* expression.

C. Representative images of wild type embryos treated +/- CVT-10216 during development (embryonic melanocytes) or in an McSC regeneration assay. Regenerated melanocytes were quantified within a consistent region delineated by the magenta dotted line on the non-regenerating control embryo (top). One data point plotted per embryo. Scale bar = 500 µm.

Development • Accepted manuscript

**** p<0.0001. One-way ANOVA with Tukey's multiple comparisons test. 4 experimental replicates.

D. Schematic of CRISPR-Cas9 strategy to target *aldh2.1* and *aldh2.2* with excision site between Cas9 cut sites (scissor symbols**; see Fig. S1)**. Wild type or *aldh2-/-* embryos in normal development, or a McSC regeneration assay shown. **** p<0.0001. Unpaired two-tailed t-test performed to calculate statistical significance. One data point plotted per embryo, 3 experimental replicates.

Development • Accepted manuscript

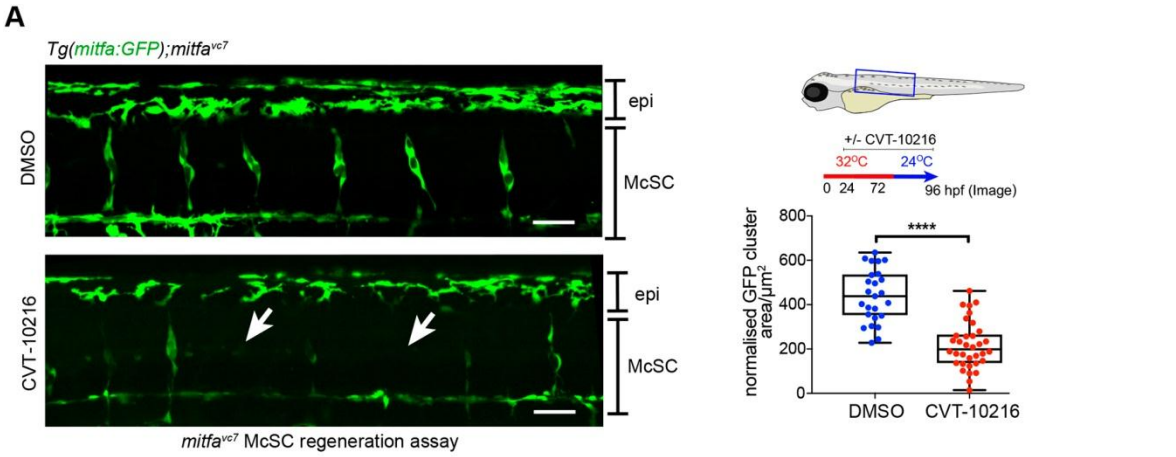

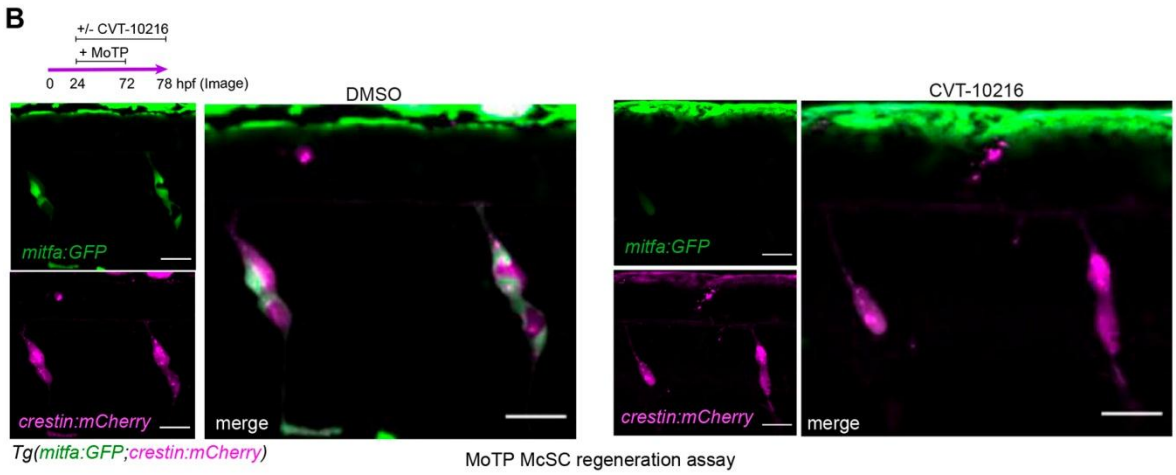

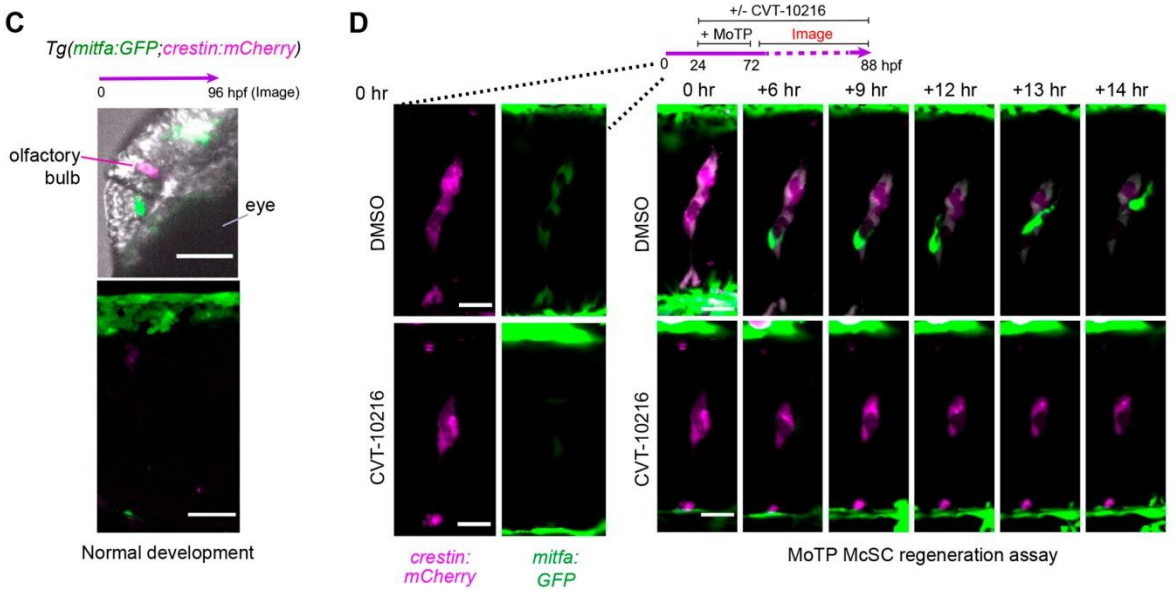

Development • Accepted manuscript

Figure 2: Live imaging captures the McSC requirement for Aldh2 to generate progeny

A. ALDH2 inhibitor (CVT-10216) causes loss of *mitfa:GFP* expression in McSCs, while dorsal stripe epithelial (epi) *GFP*+ melanoblasts remain. Representative confocal stack images of McSCs at the niche after 24 hours regeneration +/- CVT-10216 treatment. The average *mitfa:GFP* niche area μm^2/somite was quantified per embryo (one data point). McSCs with very low to no GFP signal are arrowed. Scale bars are 50 μm, 3 experimental replicates.**** $p<0.0001$. Unpaired, two-tailed t-test.

B. McSCs maintain neural crest identity when treated with ALDH2 inhibitor (CVT-10216). Confocal stack images of McSC niches in CVT-10216 treated *Tg(mitfa:GFP;crestin:mCherry)* embryos after 6 hours washout of MoTP. 2 experimental replicates, >5 embryos used per condition, representative images shown. Scale bars = 50 μm

C. 96 hpf non-regenerating *Tg(mitfa:GFP;crestin:mCherry)* embryos (same age as **B**) still express *crestin:mCherry* in the olfactory bulb and *mitfa:GFP* in embryonic epithelial melanoblasts (labelled in head, top image, and trunk bottom image), but no longer express these transgenes in McSC niches. Representative images of 3 embryos shown. Scale bars = 50 μm

D. Time lapse stills of individual regenerating McSCs at the niches. *Tg(mitfa:GFP; crestin:mCherry)* embryos with or without CVT-1016 were imaged from 2 hours post-MoTP washout. In a control embryo, an McSC undergoes cell division and a new *mitfa:GFP-high* cell migrates upwards towards the epidermis (see **Movie S3**). In a CVT-10216 treated embryo, *mitfa:GFP* expression is absent, and migration not observed (see **Movie S4**). Scale bars = 20 μm.

Development • Accepted manuscript

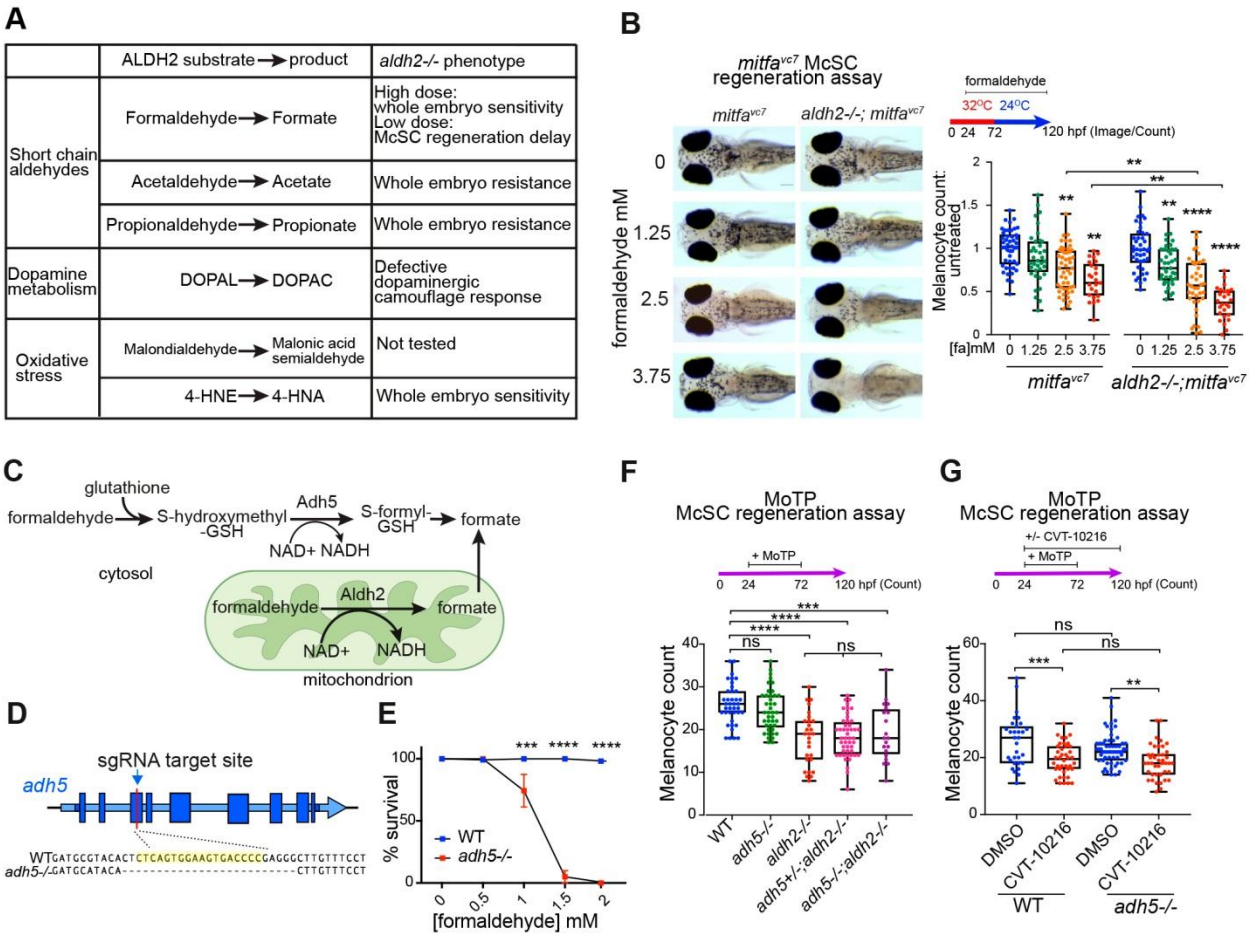

Figure 3: McSCs require Aldh2, but not Adh5, for formaldehyde metabolism

A. Table of known ALDH2 substrates and their effects on *aldh2-/-* embryos (See **Fig. S3**).

B. Melanocyte regeneration is sensitive to formaldehyde and this effect is stronger in *aldh2-/-* mutants. Images and quantification of melanocytes in zebrafish embryos in a *mitfa*^{vc7} regeneration assay. Melanocyte counts were normalised to the mean of respective control, each dot represents a single embryo, 3 experimental replicates. ** p<0.0021, **** p<0.0001. One-way ANOVA with Tukey's multiple comparisons.

C. Schematic diagram of formaldehyde metabolism by Adh5 (cytosol) and Aldh2 (mitochondria).

D. Schematic diagram showing *adh5-/-* CRISPR-Cas9 mutant, with sgRNA target site in exon 3 and alignment to WT sequence showing a deletion of 25 bp.

Development • Accepted manuscript

E. Sensitivity of *adh5-/-* embryos to increasing concentrations of formaldehyde from 24hpf for 24 hours, and surviving embryos quantified. 5 experimental replicates, 20 embryos per condition. ***p<0.0002 **** p<0.0001 Two way ANOVA with Sidak's multiple comparisons, error bars = mean±s.e.m.

F. MoTP regeneration assay on *aldh2-/-*, *adh5-/-* mutant embryos and embryos from an incross of *adh5+/-; aldh2-/-* fish (embryos genotyped after counting). One data point plotted per embryo, 3 experimental replicates. *** p<0.0002, **** p<0.0001, ns not significant. One way ANOVA with Tukey's multiple comparisons.

G. MoTP Regeneration assay on wild type and *adh5-/-* mutants treated +/- CVT-10216. One data point plotted per embryo, 3 experimental replicates. *** p<0.0002, ** p<0.0021, ns: not significant. One way ANOVA with Tukey's multiple comparisons.

Development • Accepted manuscript

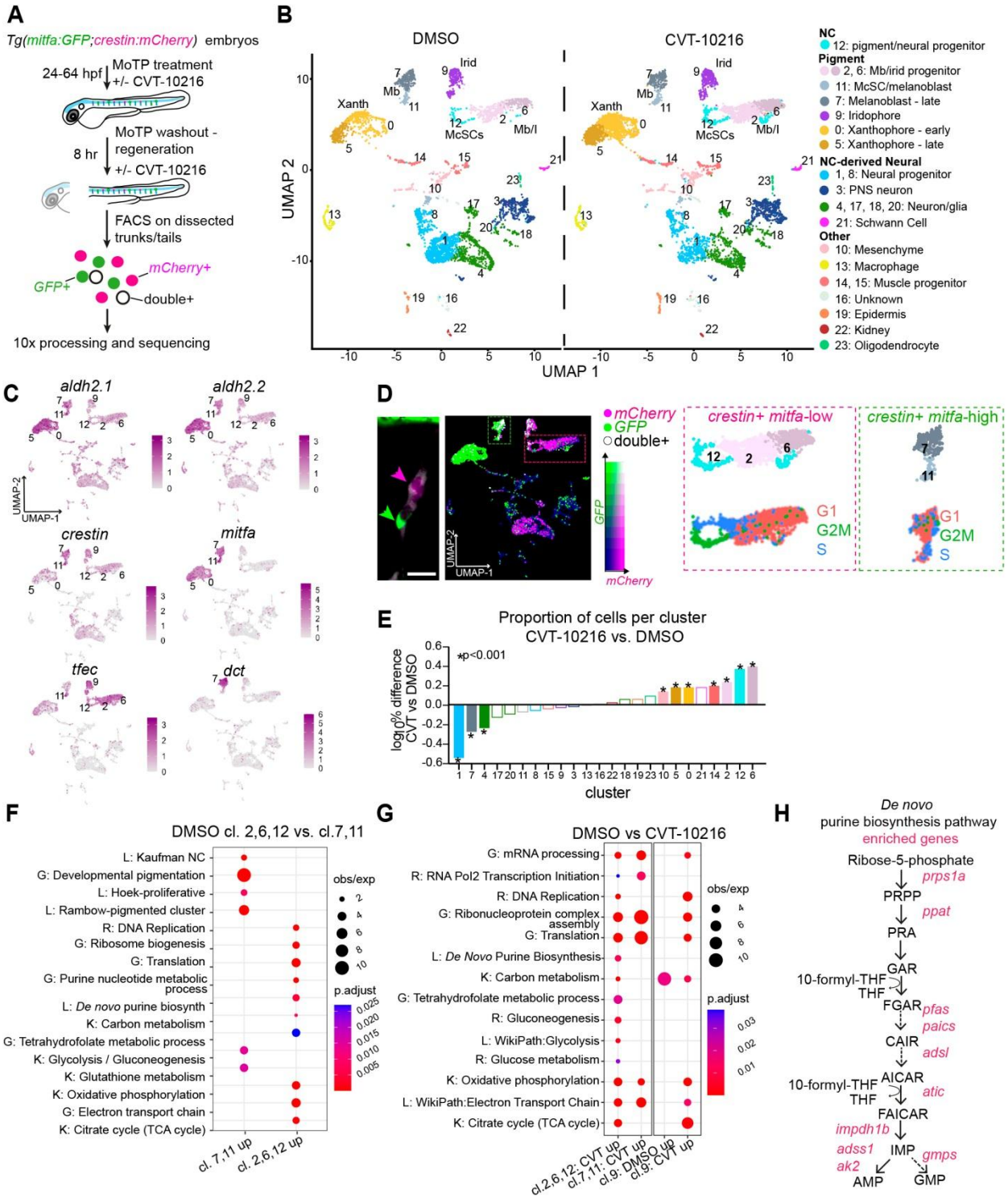

Development • Accepted manuscript

Figure 4: scRNA-seq reveals an Aldh2 metabolic gatekeeper function

A. Experimental design for the scRNA-seq experiment to capture the McSCs in regeneration.

B. UMAPs of *Tg(crestin:mCherry, mitfa:GFP)* positive cells after clustering, split by drug treatment. Mb = melanoblasts, Xanth = xanthophores, Irid = iridophores.

C. UMAPs of both DMSO- and CVT-10216 treated cells with color change from grey (negative) to purple based on $\log_2$ expression of *aldh2.1* and *aldh2.2* in pigment lineages compared to *crestin* (neural crest), *tfec* (melanophore/iridophore progenitors), *mitfa* (early melanoblasts) and *dct* (late melanoblasts).

D. Proposed relation of imaged McSCs to scRNA-seq clusters, using an example niche from **Fig. 2D** (scale bar 20 μm) and UMAP coloured by expression intensity of *mCherry* (magenta), *GFP* (green) and cells in which both are expressed (white). We predict *crestin+ mitfa-high* cells (green arrow/box) are represented in clusters 7, 11, and *crestin+ mitfa-low* cells (magenta arrow/box) are represented in clusters 2,6,12. UMAPs of these clusters (top) and their predicted cell cycle phase (bottom) are shown.

E. The proportion of total cells within each cluster compared between treatment conditions. The $\log_{10}$ percentage difference of numbers of cells in the CVT-10216 treated clusters compared to DMSO equivalents was plotted, with asterisks indicating a significant difference in proportions (Chi squared test).

F. Dot-plot of pathway analysis showing selection of significantly upregulated GO (G), KEGG (K), Reactome (R) and Literature-based (L) terms in clusters 2,6,12 compared to 7,11, and vice versa. Dot size represents observed/expected ratio, and colour adjusted p-value (Benjamini–Hochberg test).

G. As **F**, but showing significant enrichment of pathways in CVT-10216 treated cells relative to DMSO from clusters 2,6,12 (*crestin+ mitfa-low)*, clusters 7,11 (*crestin+ mitfa-high)*, and cluster 9 (predicted iridophores).

H. Schematic diagram of *de novo* purine biosynthesis, with genes encoding enzymes significantly upregulated in the CVT-10216 dataset from **G** shown in red.

Development • Accepted manuscript

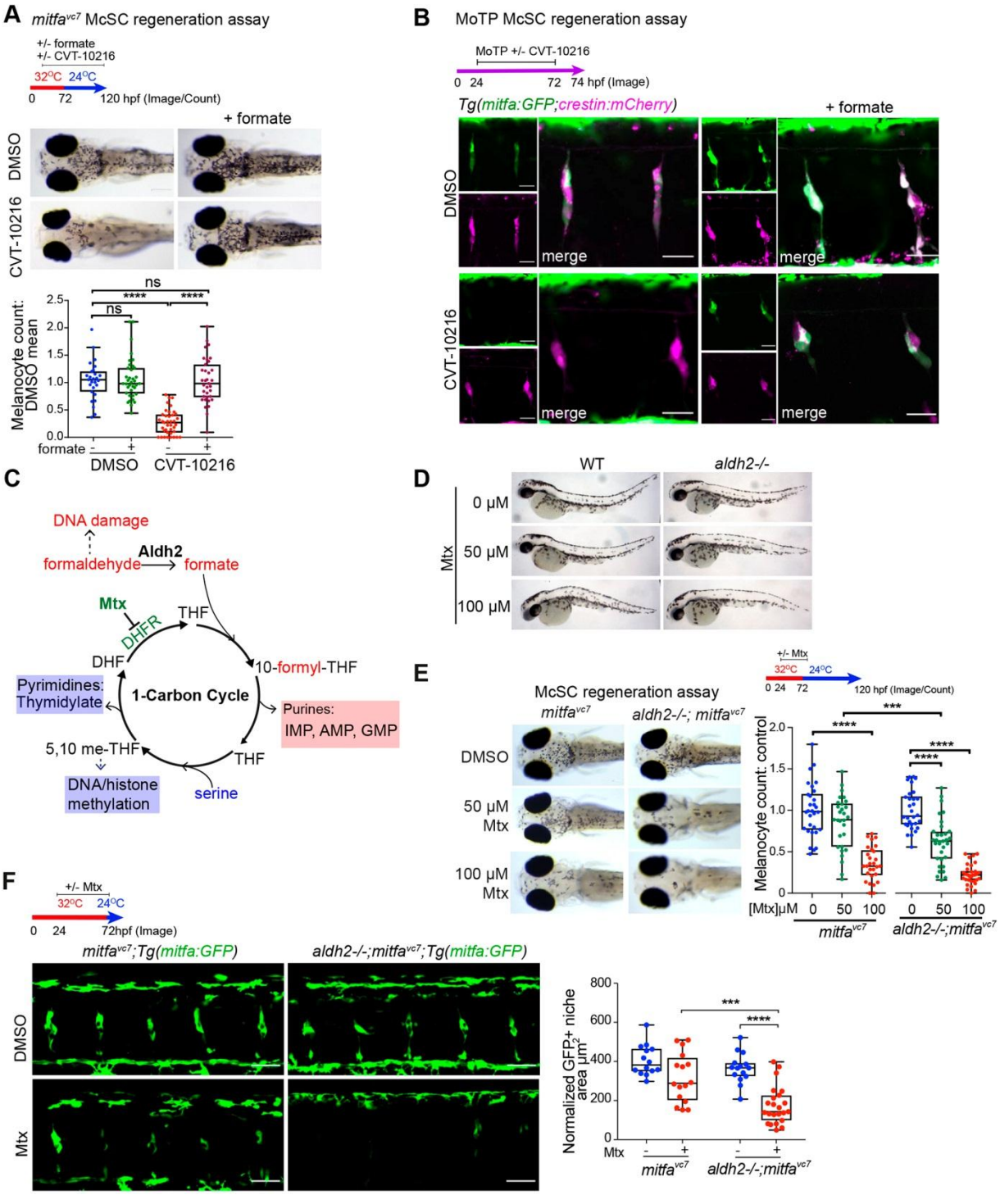

Development • Accepted manuscript

Figure 5. The Aldh2 metabolic reaction product, formate, promotes McSC-derived progeny

A. Representative images of a regeneration assay where control or CVT-10216-treated embryos were supplemented with 25 mM sodium formate. P value: **** p<0.0001, ns= not significant. Kruskall-Wallis test with Dunn's multiple comparisons. One data point per embryo, 3 experimental replicates.

B. An MoTP assay on *Tg(mitfa:GFP;crestin:mCherry)* embryos treated with or without CVT-10216 +/- 25 mM sodium formate from 24hpf. MoTP was washed out at 72hpf, and embryos imaged confocally at 74hpf. 2 experimental replicates, >5 embryos imaged per replicate. Scale bars are 25 μm. Single channel images of *crestin:mCherry* expression (magenta) and *mitfa:GFP* expression (green) are shown alongside merged.

C. Schematic of 1C metabolism and proposed function for Aldh2 formate supply through formaldehyde metabolism (based on Burgos-Barragan et al., 2017). Tetrahydrofolate (THF) combines with formate to make 10-formyl-THF, which provides two carbons to make purine nucleosides.

D. Mtx treatment has no effect on embryonic melanocytes. Zebrafish embryos (wildtype and *aldh2-/-*) treated with or without Mtx at 24 hpf for 48 hr. N=3.

E. Representative images of control and *aldh2-/-* mutants +/- Mtx treatment in a *mitfa*^{vc7} regeneration assay. The melanocyte count at each dose was normalised to its respective DMSO control. Each dot represents a single embryo. *** p<0.0002, **** p<0.0001. One-way ANOVA performed with Tukey's multiple comparisons test. One data point plotted per embryo, 3 experimental replicates.

F. Confocal Z-stacks of *mitfa:GFP* McSCs in a *mitfa*^{vc7} regeneration assay, in control or *aldh2-/-* embryos treated with or without Mtx. Scale bars are 50 μm. 2 experimental replicates, >5 embryos imaged per repeat. Quantification of GFP+ niche area/somite of embryos treated with Mtx is shown. *** p<0.0002, **** p<0.0001. One-way ANOVA with Tukey's multiple comparisons.

Development • Accepted manuscript

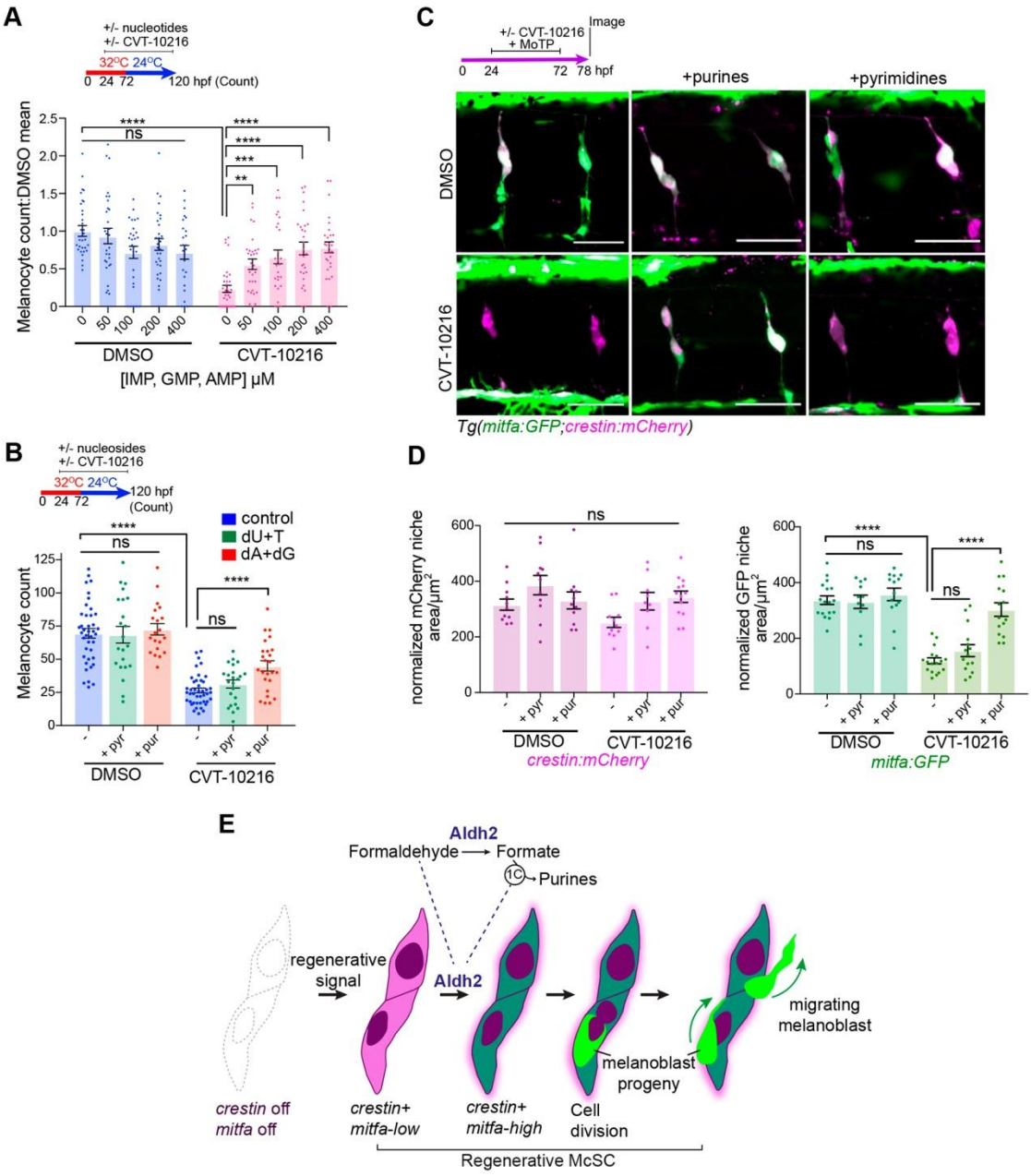

Figure 6: Aldh2 meets the demand of McSCs for purines

A. Purine nucleotides rescue Aldh2-deficient melanocyte regeneration. Melanocyte regeneration assay in *mitfa*^{vc7} embryos +/- CVT-10216 plus purine nucleotide cocktail. Melanocyte counts normalized to respective untreated controls. Each dot represents a single embryo, 3 experimental replicates, error bars = mean±s.e.m. ** p<0.0021, *** p<0.0002, **** p<0.0001, ns= not significant. One-way ANOVA with Tukey's multiple comparisons.

Development • Accepted manuscript

B. Purine, but not pyrimidine nucleosides, rescue Aldh2-deficient melanocyte regeneration. Melanocyte regeneration assay on *mitfa*^{vc7} embryos +/- CVT-10216 and supplemented with deoxyadenosine (dA), deoxguanosine (dG), or deoxyuridine (dU) or thymidine (T) nucleosides (200 µM). Each datapoint represents a single embryo, 3 experimental replicates. **** p<0.0001, ns= not significant, error bars = mean±s.e.m. One-way ANOVA with Tukey's multiple comparisons.

C. Purine nucleotides rescue McSC differentiation in ALDH2i-treated embryos. Representative confocal Z-stacks of *Tg(mitfa:GFP;crestin:mCherry)* embryos treated with MoTP +/- CVT-12016, as well as 400 µM AMP/GMP purine nucleotides, or 400 µM UMP/Thymidine pyrimidine nucleotides. 2 experimental replicates, >5 embryos per condition.

D. Quantification of *crestin:mCherry* and *mitfa:GFP* niche areas from **C**. Each dot represents the sum of the GFP or mCherry niche area/ number of somites in view in one embryo. ****:p<0.0001, ns: not significant. Error bars = mean±s.e.m. One-way ANOVA with Tukey's multiple comparisons.

E. Proposed model for Aldh2 control of the McSC lineage. Regenerating McSCs start expressing *crestin* and low levels of *mitfa*. Next, McSCs increase their metabolic demands for purine nucleotides to express high levels of *mitfa* and generate progeny. This metabolic demand is met by Aldh2 metabolizing endogenous formaldehyde into formate, which is then used in the 1C cycle to fuel production of purine nucleotides. McSCs undergo cell division to generate progeny, which migrate away from the niche to the epidermis. ALDH2i (CVT-10216) delays the progression of the activated McSC to generate progeny in regeneration.

Development • Accepted manuscript

Brunsdon *et al.*, Supplemental Figure S1

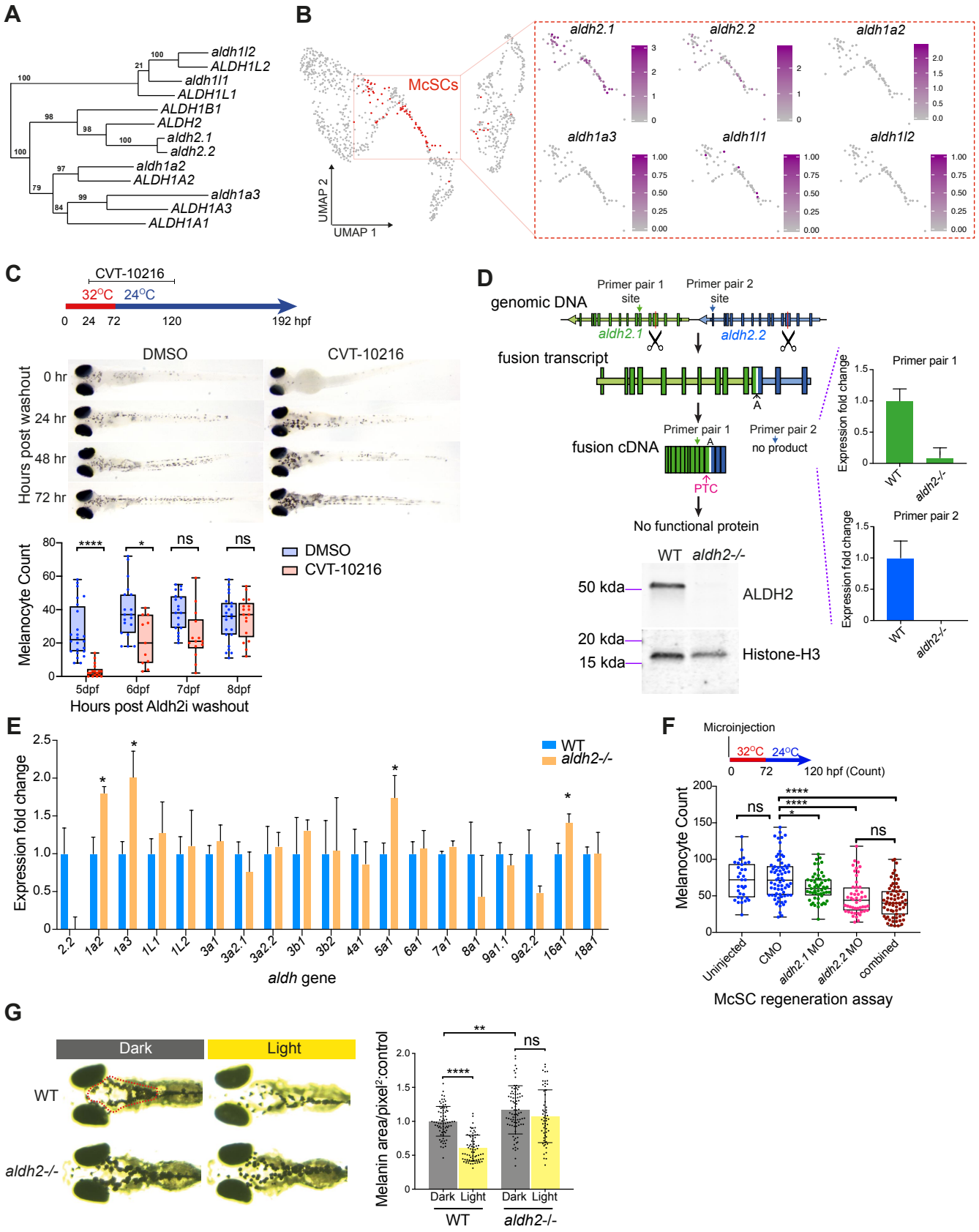

Development • Supplementary information

Fig. S1. *aldh gene* expression in the McSC lineage and Aldh2 loss of activity assays

A. Phylogenetic tree showing the relationship between human *ALDH* and zebrafish *aldh* genes from the ALDH1 and ALDH2 families.

B. As **Fig. 1A**, but showing expression levels of *aldh1* family genes.

C. Extended regeneration assay on *mitfa*^{vc7} embryos following CVT-10216 treatment between 24-120hpf. After washout, larvae were imaged and melanocytes quantified each day. Representative images shown. Each datapoint represents a single larva, 3 experimental replicates. *: p<0.0332, ****: p<0.0001, ns: not significant. Kruskal-Wallis test with Dunn's multiple comparisons.

D. sgRNAs targeting exon 3 of *aldh2.1* and *aldh2.2* were co-injected with Cas9, causing deletion of the intergenic region and creation of a fusion transcript, containing a 1 bp insertion and premature termination codon (PTC). RT-qPCR was performed with primers targeting Primer site 1, persisting in the truncated fusion transcript, and Primer site 2 (excised), see Methods. Housekeeping control: *β-actin*. 3 experimental replicates. Error bars = mean±s.e.m. Western blot analysis of ALDH2 protein in *aldh2-/-* and WT embryos confirms a lack of Aldh2 protein in mutants. Loading control: Histone-H3.

E. RT-qPCR showing *aldh2.2* expression levels relative to other *aldh* genes in 72hpf WT or *aldh2-/-* mutant embryos, normalized to *β-actin*. 3 experimental replicates. Error bars = mean±s.e.m. Asterisks mark *aldh* genes upregulated >1.5-fold in *aldh2-/-* mutants.

F. Regeneration assay on *mitfa*^{vc7} embryos injected with 6 ng of standard control morpholino (CMO), or morpholinos against either/both *aldh2.1* and *aldh2.2*. Regenerated melanocytes are quantified, each datapoint represents a single embryo, 3 experimental replicates. * p<0.0332, **** p<0.0001, ns: not significant. One-way ANOVA with Tukey's multiple comparisons.

G. Representative images shown of embryos after adaptation to dark or light surroundings. Melanin coverage within the red outlined area was quantified. N=3 biological replicates. Error bars = mean±s.d. **: p<0.0021, ****: p<0.0001. One-way ANOVA with Tukey's multiple comparisons.

Development • Supplementary information

Brunsdon *et al.*, Supplemental Figure S2

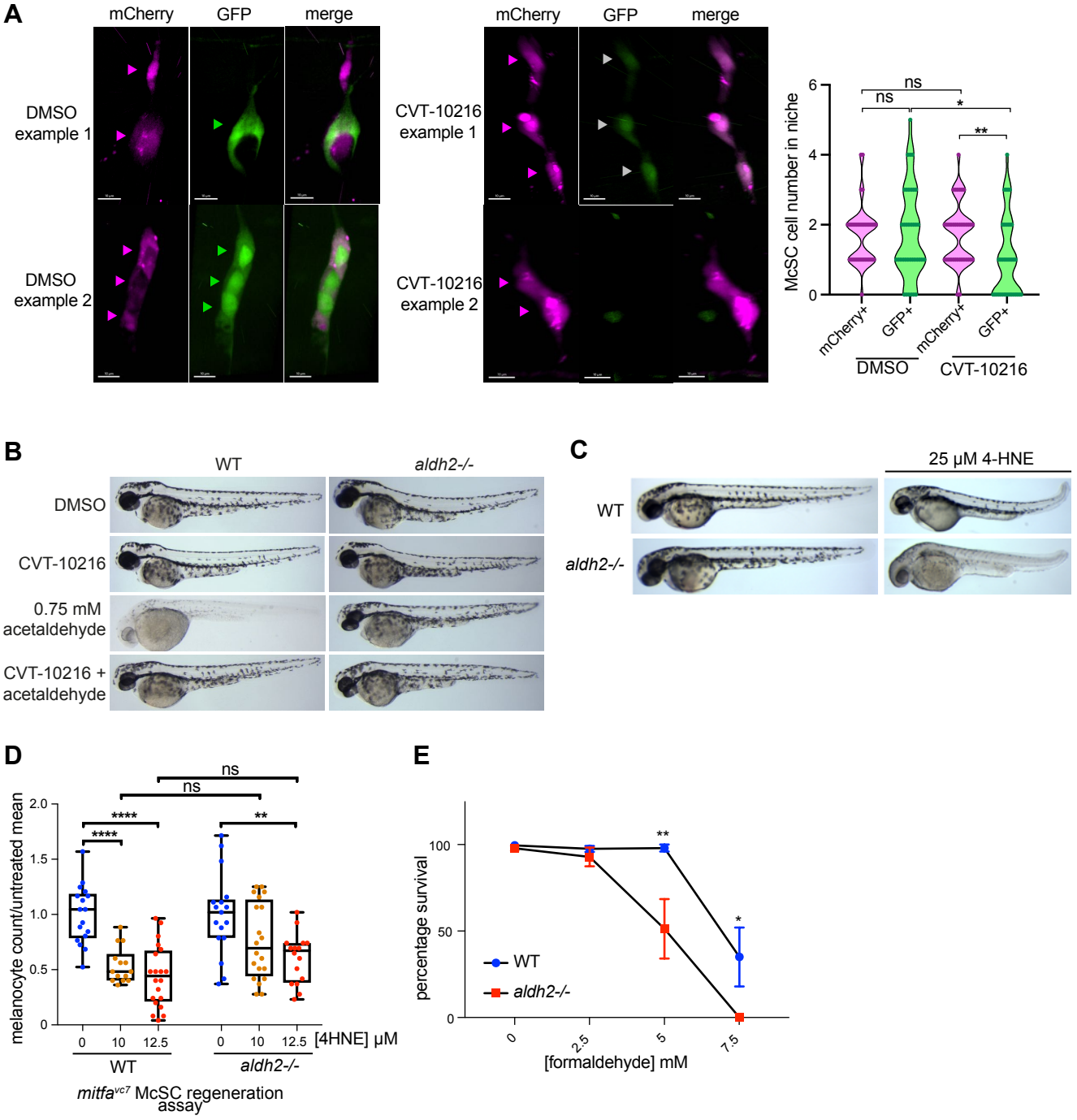

Development • Supplementary information

Fig. S2. Results of aldehyde screen on *aldh2-/-* mutant zebrafish

A. Left: Static images from Movie S1 and S2 (bottom row) plus two additional example McSC niches showing individual *crestin:mCherry* and *mitfa:GFP*-expressing cells (arrowed) during regeneration in embryos treated with either DMSO or CVT-10216, scale bars 10 µm. GFP fluorescence is fainter (gray arrows) or missing after CVT-10216 treatment. Right: Quantification of mCherry+ and GFP+ cells in each niche (3 niches imaged in 12 embryos per condition). Each dot represents a single niche. **: $p<0.0021$, *:$p<0.03$. Kruskall-Wallis test with Dunn's multiple comparisons.

B. Representative images of 72hpf WT and *aldh2-/-* mutant embryos treated with 0.75 mM acetaldehyde with or without CVT-10216. Unexpectedly, Aldh2 loss or deficiency confers resistance to acetaldehyde. 3 experimental replicates, >8 embryos per condition.

C. Representative images of 72hpf WT and *aldh2-/-* mutant embryos treated with 25 µM 4-HNE, showing whole body sensitivity in the mutant. 2 experimental replicates, 15 embryos per condition.

D. *mitfa*^{vc7} melanocyte regeneration assay and subsequent quantification of embryos treated with increasing doses of 4-HNE, showing no significant difference between controls and *aldh2-/-; mitfa*^{vc7} embryos in terms of reduction in regeneration potential after 4-HNE treatment. For comparison between genotypes, melanocyte numbers were normalized to the average untreated condition for each genotype. 2 experimental replicates, each datapoint represents a single embryo. ** $p<0.0021$, **** $p<0.0001$, ns not significant. One-way ANOVA with Tukey's multiple comparisons.

E. Survival percentage of WT and *aldh2-/-* mutant embryos treated with various concentrations of formaldehyde. 6 experimental replicates, 20 embryos per condition. Error bars = mean±s.e.m. ** $p<0.0021$. Two way ANOVA with Sidak's multiple comparisons.

Development • Supplementary information

Brunsdon *et al.*, Supplemental Figure S3

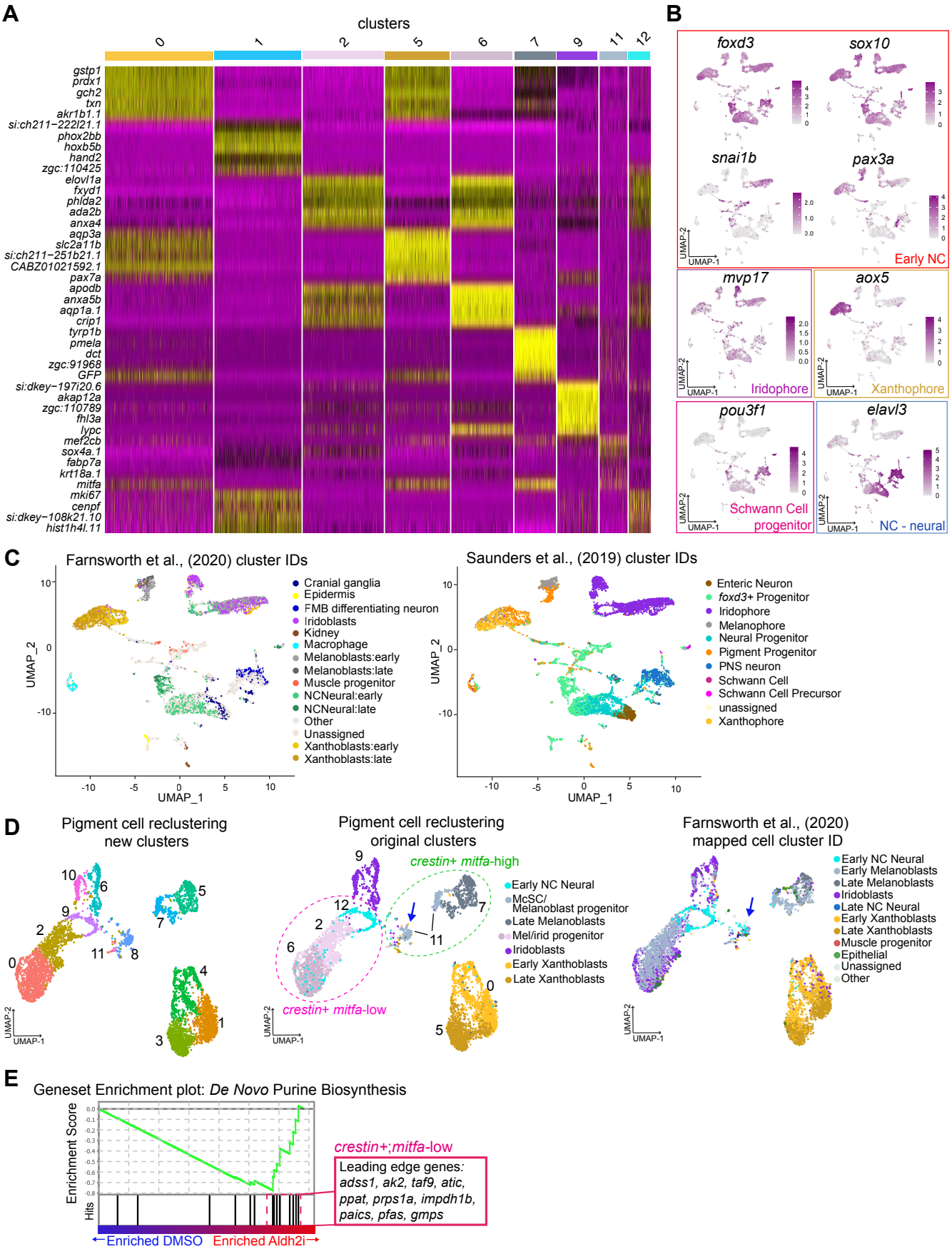

Development • Supplementary information

Fig. S3. Identification of transcriptionally distinct scRNA-seq clusters during McSC regeneration

A. Heatmap showing top 5 cluster-defining genes per selected clusters.

B. UMAP of the combined dataset showing gene expression of early neural crest markers, and non-pigment clusters marked by *pou3f1* (Schwann Cell Progenitors), *mcamb* and *elavl3* marking NC-derived neural cells, *mvp17* marking iridophores, and *aox5* marking xanthophores.

C. UMAP of this scRNA seq data mapped with cell identity annotation from Farnsworth et al (2020) and Saunders et al (2019).

D. Left: UMAP of the combined dataset subsetted by the pigment cells and reclustered into 12 clusters. Center: UMAP annotated with the original clusters, showing the *crestin+;mitfa*-high and *crestin+;mitfa*-low McSCs and split cluster 11. Right: overlap with Farnsworth clusters, showing a portion of original cluster 11 containing a range of neural and pigment cell identities.

E. GSEA enrichment plot of the *de novo* purine biosynthesis signature upregulated in clusters 2,6,12 in CVT-10216 treated embryos compared to control, generated using the Deseq2 output ranked by the Deseq2 test statistic. The green line and y-axis represent the enrichment score of the pathway, that is, the extent of correlation between the DMSO dataset to *de novo* purine synthesis, relative to the Aldh2i dataset. Individual genes within this pathway are represented as vertical black lines, with genes contributing most towards the result - NES -1.18, FDR <25% (Kolganov Smirnov test) - boxed and listed to the right.

Development • Supplementary information

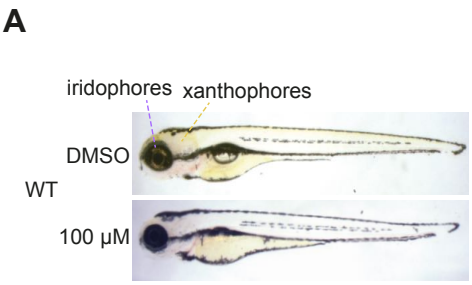

Fig. S4. Validation of Mtx treatment

A. Mtx treated embryos (96 hpf) have lost reflective iridophore pigments (clearly observed in the eye) and yellow xanthophore pigments.

Table S1. scRNA-seq: top 30 cluster markers

Click here to download Table S1

Table S2. scRNA-seq: metrics, clustering information and cell states

Click here to download Table S2

Table S3. Differential expression analysis of *crestin+ mitfa-low* vs *crestin+ mitfa-high* cells

Click here to download Table S3

Development • Supplementary information

Table S4. Differential expression analysis of *crestin+ mitfa-low* cells, DMSO vs CVT-10216

Click here to download Table S4

Table S5. Differential expression analysis of *crestin+ mitfa-high* cells, DMSO vs CVT-10216

Click here to download Table S5

Table S6. Differential expression analysis of iridophore cluster 9, DMSO vs CVT-10216

Click here to download Table S6

Table S7. Oligonucleotide sequences

Click here to download Table S7

Development • Supplementary information

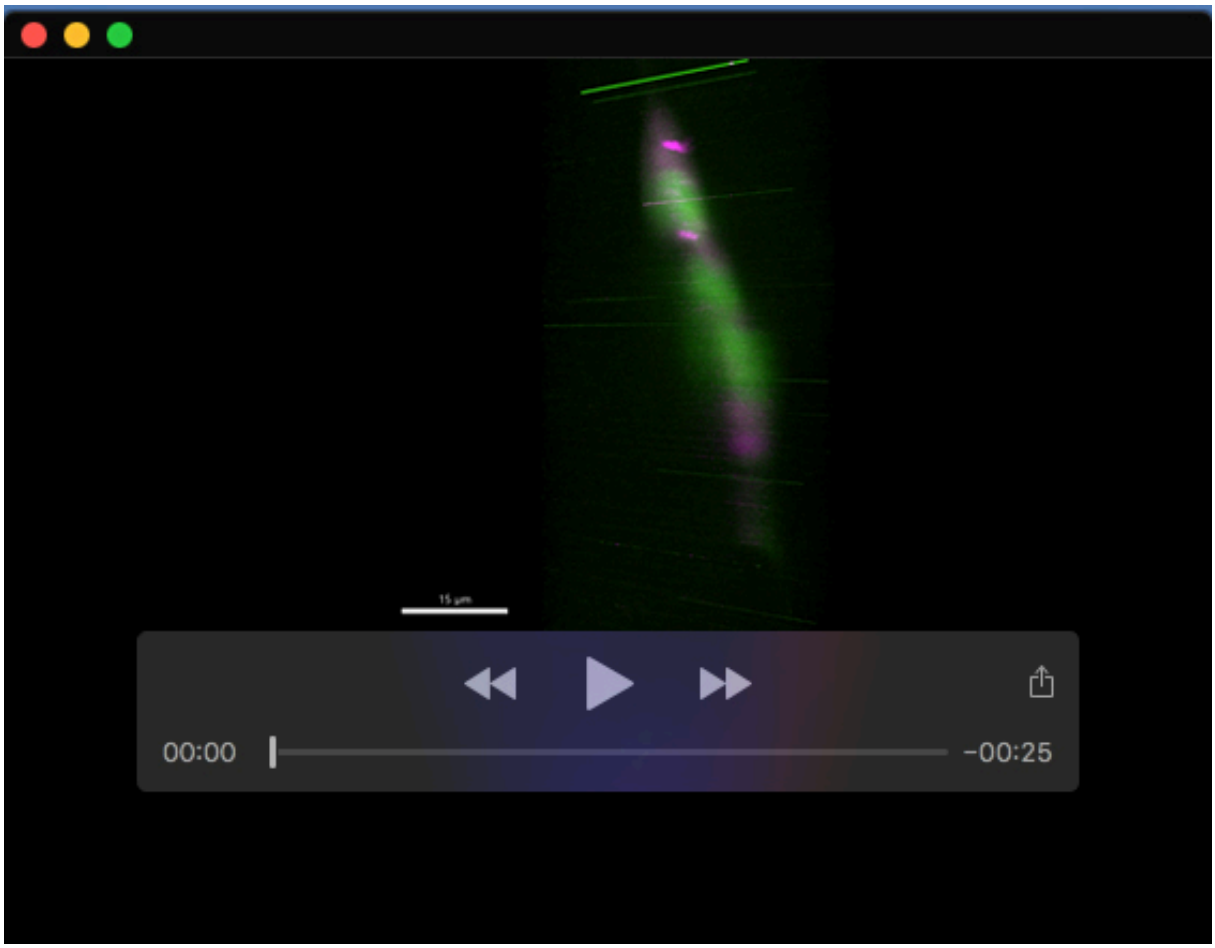

Movie 1. McSCs in a regenerating embryo (DMSO control)

Movie showing 3D rendering of a representative McSC cluster during regeneration. Here, an embryo expressing transgenes *crestin:mCherry* and *mitfa:GFP* embryo is imaged at the onset of regeneration following MoTP treatment. In this example, three cells in the McSC niche express both *GFP* and *mCherry*. See **Fig. S2**, DMSO example 2

Development • Supplementary information

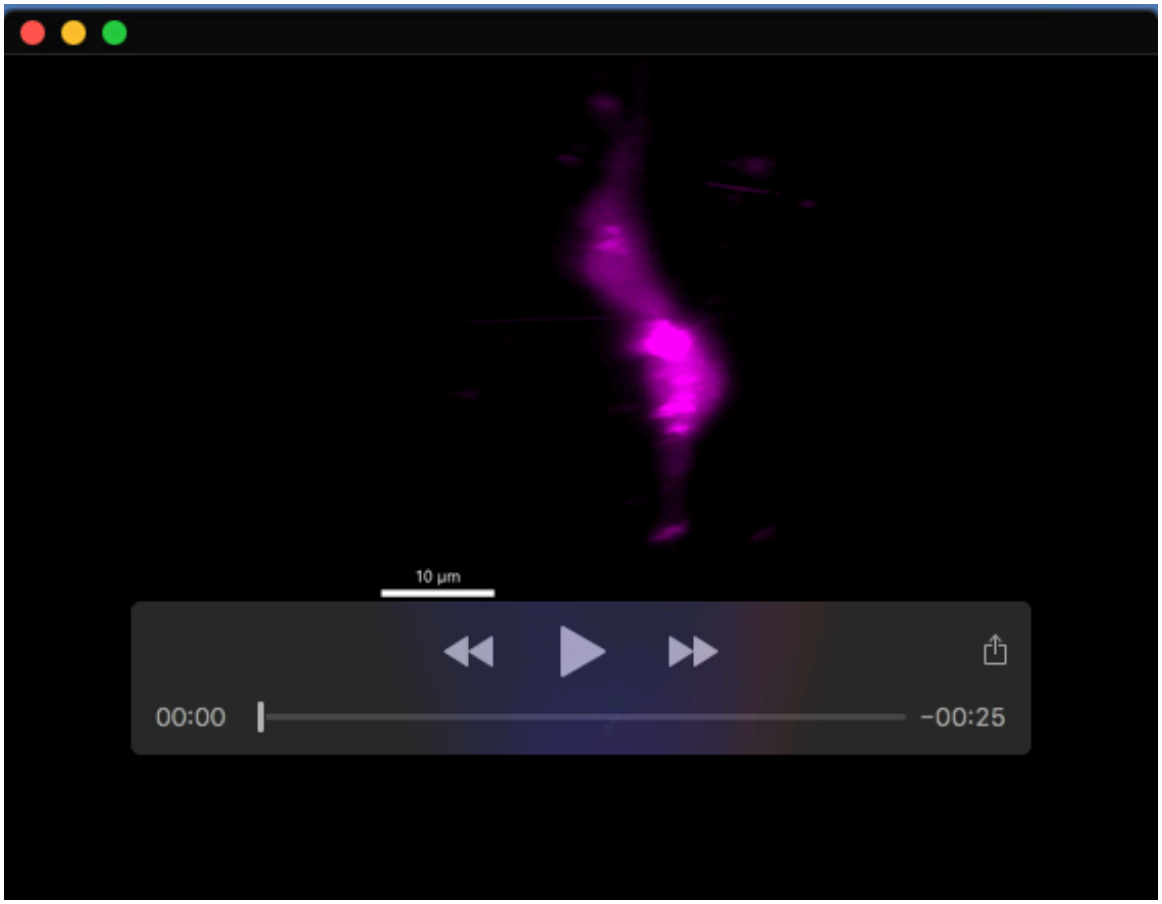

Movie 2. McSCs in a regenerating embryo following ALDH2 inhibitor (CVT-10216) treatment.

Movie showing 3D rendering of a representative McSC cluster during regeneration. Here, an embryo expressing transgenes *crestin:mCherry* and *mitfa:GFP* embryo is imaged at the onset of regeneration during CVT-10216 treatment and following MoTP treatment. In this example, two cells express *mCherry*, but while GFP is detected in a neighbouring cell, it is not expressed in this McSC niche. See **Fig. S2**, CVT-10216 example 2.

Development • Supplementary information

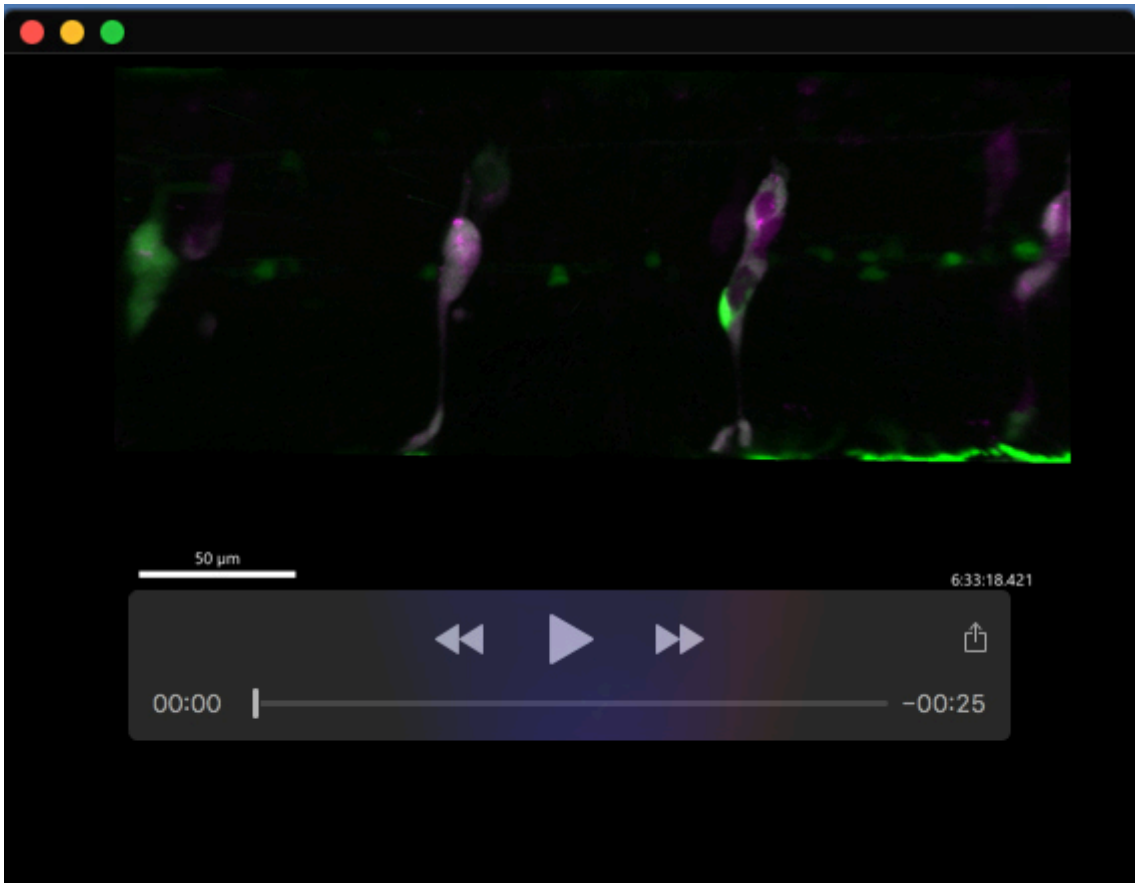

Movie 3. McSCs generate progeny

Time-lapse video of a *Tg(crestin:mCherry;mitfa:GFP)* embryo during McSC regeneration (DMSO control). Embryos were treated with MoTP to kill differentiated melanocytes and initiate melanocyte regeneration. McSCs were followed for over 14 hours (post MoTP washout). McSCs are *crestin+ mitfa-low*, but then during or shortly after cell division, a cell strongly expresses GFP+ to become a *mitfa-high* cell, which then leaves the McSC compartment and migrates towards the epidermis.

Development • Supplementary information

Movie 4. Aldh2i inhibits McSCs ability to generate progeny

Time-lapse video of a *Tg(crestin:mCherry;mitfa:GFP)* embryo during McSC regeneration in the presence of ALDH2i. Embryos were treated with CVT-10216 to inhibit Aldh2, and co-treated with MoTP to kill differentiated melanocytes, and initiate melanocyte regeneration. McSCs were followed for over 14 hours (post MoTP washout, but in the presence of ALDH2i).

Development • Supplementary information